polymers

MDPI

Article

Antifungal Effects of Curcumin- and Quercetin-Loaded Polyvinyl Alcohol–Cinnamyl Chitosan Hybrid Nanoparticles

Emre Karaduman [1], Ozlem Tavukcuoglu [2], Deniz Tigli Torun [3], Ahmet Akif Kızılkurtlu [4,*], Ali Can Özarslan [5] and Fatih Ciftci [6,7,8]

1 Department of Bioengineering, Faculty of Chemical and Metallurgical Engineering, Yildiz Technical University, Istanbul 34220, Turkey; emrkrdmn@gmail.com
2 Department of Biochemistry, Faculty of Hamidiye Pharmacy, University of Health Sciences, Istanbul 34668, Turkey; ozlemoztolan@gmail.com
3 Department of Nutrition and Dietetic, Istanbul Kent University, Istanbul 34433, Turkey; dytdeniztigli@gmail.com
4 Department of Biomedical Engineering, Faculty of Engineering and Natural Sciences, Atlas University, Istanbul 34408, Turkey
5 Department of Metallurgical and Materials Engineering, Faculty of Engineering, Istanbul University-Cerrahpasa, Istanbul 34320, Turkey; alicanozarslan@gmail.com
6 Department of Biomedical Engineering, Faculty of Engineering, Fatih Sultan Mehmet Vakıf University, Istanbul 34015, Turkey; fciftci@fsm.edu.tr
7 Biomedical Electronic Design Application and Research Center (BETAM), Fatih Sultan Mehmet Vakıf University, Istanbul 34015, Turkey
8 BioriginAI Research Group, Department of Biomedical Engineering, Fatih Sultan Mehmet Vakıf University, Istanbul 34015, Turkey
* Correspondence: ahmet.kizilkurtlu@atlas.edu.tr

Abstract

Novel hybrid nanoparticles integrating polyvinyl alcohol (PVA) and cinnamyl-functionalized chitosan (Cin-Ch) within an ionically crosslinked polymer network were synthesized and characterized for the controlled delivery of curcumin (CUR) and quercetin (QC). Reductive amination achieved an isolated gravimetric reaction yield of 78.4% ± 3.2% and a degree of substitution (DS) of approximately 18%, as cross-validated orthogonally via elemental microanalysis (DS_{EA} = 18.2%, atomic C/N shift from 5.16 ± 0.04 to 6.85 ± 0.05), solution-state ^{1}H NMR (DS_{NMR} = 18.0%, *trans*-stereochemistry J = 15.8 Hz), and TNBS colorimetric titration (DS_{TNBS} = 18.1% ± 0.3%, CV = 1.33%). Cinnamyl grafting altered macromolecular polarity, elevating the static water contact angle from 93.2° ± 2.1° to 107.4° ± 2.4° ($p < 0.001$), while XPS core-level deconvolution corroborated successful covalent conjugation through the emergence of a secondary amine bridge (–NH–CH_2– at 399.4 eV, 52.4% of total N 1s) and an aromatic $\pi \rightarrow \pi^*$ shake-up satellite at 291.2 eV. Under optimized DMSO-based ionic gelation conditions without surfactants, the hybrid nanoparticles achieved encapsulation efficiencies exceeding 99.8% (99.99% for CUR; 99.85% for QC) and loading capacities of 64.8% and 57.3%, respectively. Dynamic light scattering revealed unimodal, submicron hydrodynamic diameters (200.2 nm, PDI = 0.240 for PVA–Cin-Ch–Cur; 197.3 nm, PDI = 0.250 for PVA–Cin-Ch–Quer), which remained colloidally stable at 4 °C over 14 days without macroscopic aggregation. Electrophoretic mobility indicated a modulated surface charge (ζ = +9.25 mV and +8.76 mV), where physical suspension stability was predominantly maintained by the steric hydration layer of PVA. In vitro release profiling in hydroalcoholic buffer over 24 h demonstrated that cinnamyl functionalization significantly suppressed the rapid burst release characteristic of native chitosan nanoparticles (>86–92% within 8 h), transitioning the kinetics into a sustained biphasic diffusion regime (62.3% ± 2.0% for CUR and 75.8% ± 2.1% for QC at 24 h). Broth microdilution assays corroborated by resazurin metabolic profiling demonstrated potent synergistic antifungal inhibition:

Check for updates

Academic Editor: Emilio Bucio

Received: 5 October 2026
Revised: 2 November 2026
Accepted: 6 November 2026
Published: 16 November 2026

Copyright: © 2026 by the authors. Licensee MDPI, Basel, Switzerland. This article is an open access article distributed under the terms and conditions of the Creative Commons Attribution (CC BY) license.

PVA–Cin-Ch–Cur and PVA–Cin-Ch–Quer reduced the Minimum Inhibitory Concentrations (MICs) to 62.5 ppm and 46.8 ppm against *Penicillium digitatum*, and to 125 ppm and 93.7 ppm against *Aspergillus niger*, outperforming free bioactives (MIC = 1666–2500 ppm), native chitosan (MIC > 2500 ppm), and unmodified chitosan nanoparticles (MIC = 416–833 ppm). These findings establish the PVA–Cin-Ch hybrid nanocomposite platform as an effective, reproducible nanocarrier system for the stabilization and sustained delivery of hydrophobic polyphenolic antimicrobials.

Keywords: chitosan; curcumin; PVA; hybrid nanoparticles; antimicrobial food packaging; biocompatible platform

1. Introduction

Necrotrophic and saprophytic filamentous fungi—with *Penicillium digitatum* and *Aspergillus niger* being the most economically damaging—drive significant postharvest losses across global supply chains and compound food safety concerns [1,2]. Synthetic fungicides have long served as the frontline defense, yet decades of reliance have bred resistant fungal populations, left persistent chemical residues in soil and water, and raised serious toxicological flags for non-target species [3,4]. This trajectory has redirected attention toward naturally occurring polyphenols. Curcumin and quercetin, for instance, disrupt fungal physiology through multiple concurrent pathways: reactive oxygen species generation, sterol biosynthesis suppression, and direct inhibition of spore germination [5–7]. The practical challenge is that these molecules are intensely hydrophobic. Poor aqueous dispersibility, rapid photodegradation, hydrolytic instability, and weak retention at the infection site all conspire to neutralize their promise under real-world agricultural conditions [8]. Engineering biocompatible colloidal carriers that can sequester these lipophilic actives and modulate their release kinetics under ambient storage conditions is therefore a prerequisite for translating polyphenol biofungicides from the laboratory to the field [9–11].

Chitosan—a linear copolymer of β-(1→4)-linked D-glucosamine and *N*-acetyl-D-glucosamine—has attracted sustained interest for antimicrobial applications owing to its film-forming ability, ready biodegradability, and inherent surface bioactivity [12,13]. Its native form, however, carries notable drawbacks. Its antifungal potency is modest on its own, and solubility drops sharply above pK_a ~ 6.5, curtailing performance in neutral or weakly acidic environments [14–16]. Chemical modification of the primary amine groups offers a direct route to rebalance the hydrophilic–lipophilic character while preserving the backbone's biodegradability [17,18]. One particularly effective approach involves Schiff base condensation of cinnamaldehyde onto the amine sites, followed by selective hydride reduction to yield cinnamyl-modified chitosan (Cin-Ch) [19–21]. The grafted phenylpropanoid side chains lower interfacial surface free energy, strengthen direct contact with fungal lipid bilayers, and—critically—convert the polysaccharide into a lipophilic matrix capable of physically entrapping hydrophobic polyphenols.

Even with favorable binding affinity, purely polysaccharide-based networks formed through ionic gelation tend to swell excessively in water, aggregate under shear, and release their payloads in an uncontrolled burst [22–24]. Blending synthetic poly(vinyl alcohol) (PVA) into the chitosan continuous phase addresses each of these failure modes [25–27]. Through intermolecular hydrogen bonding with residual polar groups on the chitosan chains, PVA constructs an interpenetrating steric barrier that restricts water ingress, curbs swelling, and shields submicron colloids from irreversible flocculation [28–30]. An additional benefit of combining non-ionic PVA with cationic chitosan is the attenuation of

excessive surface electropositivity, yielding hybrid colloids that disperse uniformly rather than self-aggregating [31,32].

How tightly an encapsulated polyphenol is held—and how quickly it diffuses out—depends fundamentally on the thermodynamic affinity between the penetrant and the surrounding polymer network [33,34]. Unmodified chitosan relies largely on transient hydrogen bonds, which offer limited retention. The cinnamyl grafts in Cin-Ch, by contrast, create localized aromatic microdomains that engage the conjugated backbones of curcumin and quercetin through π–π stacking and hydrophobic association [35,36]. These supramolecular interactions retard leaching from particle surfaces and shift the release mechanism toward a prolonged matrix-diffusion regime [37,38]. Although individual polyphenol nanoformulations have been reported in recent years [39,40], a systematic comparison of entrapment efficiency, release thermodynamics, and pathogen-inhibitory kinetics across unmodified versus cinnamyl-functionalized PVA–chitosan matrices have not yet been undertaken.

In the present study, an ionically crosslinked PVA–Cin-Ch hybrid nanoparticle platform was developed for the nanoencapsulation and sustained delivery of curcumin (PVA–Cin-Ch–Cur) and quercetin (PVA–Cin-Ch–Quer). Cinnamyl substitution degree, bond configuration, and film wettability were quantified through a combination of ^{1}HNMR, ATR-FTIR, XPS, CHNO elemental analysis, and sessile drop contact angle measurements. To eliminate spectrophotometric cross-talk between curcumin (λ = 429 nm) and quercetin (λ = 372 nm), the two bioactives were encapsulated separately. An expanded eight-group comparative design was employed to evaluate the influence of cinnamyl functionalization on entrapment efficiency, hydrodynamic particle size, 24-h in vitro release behavior, and antifungal efficacy against *Penicillium digitatum* and *Aspergillus niger*. Covalent cinnamylation, working in concert with the PVA stabilizing network, is shown to suppress burst release and significantly amplify fungal growth inhibition at active concentrations well below those required for the free compounds or unmodified polymer controls.

2. Materials and Methods

2.1. Materials

PVA (Mw ≈ 85,000 g/mol, 99% hydrolyzed) and low-molecular-weight chitosan (degree of deacetylation ≈ 76%) were obtained from Sigma-Aldrich (Darmstadt, Germany). Cinnamaldehyde and sodium borohydride ($NaBH_4$) were also purchased from Sigma-Aldrich and used for the reductive amination of chitosan. Curcumin (CUR) and quercetin (QC) (≥98% purity, Sigma-Aldrich, St. Louis, MO, USA) were used as model polyphenolic compounds for encapsulation studies. Sodium tripolyphosphate (TPP), used as an ionic crosslinker, was obtained from Sigma-Aldrich. Dimethyl sulfoxide (DMSO), ethanol, lactic acid, and methanol (analytical grade) were purchased from Merck (Darmstadt, Germany) and used as solvents for polymer dissolution, chemical modification, and polyphenol dispersion. Tween 80 and sodium bicarbonate were used without further purification. The fungal strains A. niger and P. digitatum were obtained from in-house microbial culture collections (Istanbul, Türkiye). Growth media, including Dichloran Rose Bengal Chloramphenicol (DRBC) agar, Sabouraud Dextrose Agar (SDA), and Yeast Peptone Dextrose (YPD) broth, were purchased from Merck (Germany) and Neogen (Manassas, VA, USA). Ultrapure water was obtained using a Milli-Q Direct 3 UV purification system (Millipore, Bedford, MA, USA).

2.2. Synthesis of Cin-Ch

Cin-Ch was synthesized through a reductive amination reaction based on previously reported methods with minor modifications [41,42]. Chitosan was first dissolved in 1%

(v/v) lactic acid to prepare a 1% (w/v) solution. A methanolic solution of cinnamaldehyde (2 molar equivalents relative to the glucosamine units of chitosan) was added dropwise under an argon atmosphere, and the mixture was stirred for 12 h at pH 5 to facilitate Schiff base formation between the aldehyde and amine groups. Subsequently, sodium borohydride (5 molar equivalents) was slowly added to reduce the formed imine bonds into stable secondary amines, and the reaction was allowed to proceed for an additional 24 h. The pH was then adjusted to 12 using 2 M NaOH to precipitate the modified polymer. The product was collected by centrifugation at 9000 rpm for 20 min, thoroughly washed three times with ethanol to remove unreacted reagents and by-products, and then freeze-dried to obtain the Cin-Ch powder.

2.3. Preparation of Polyphenol-Loaded PVA–Cin-Ch Hybrid Nanoparticles (PVA–Cin-Ch–Cur and PVA–Cin-Ch–Quer)

PVA stock solution was prepared at 5% (w/v) by dispersing PVA in ultrapure water and heating at 85 °C under magnetic stirring until complete dissolution. The clear solution was cooled to room temperature before use. Cin-Ch was dissolved at 0.5% (w/v) in 1% (v/v) lactic acid under gentle stirring to obtain a transparent polymer solution. PVA and Cin-Ch solutions were then combined at a volumetric ratio of 3:1 to yield the PVA–Cin-Ch hybrid matrix. Curcumin and quercetin stock solutions were prepared separately in dimethyl sulfoxide (DMSO) at 50 mg/mL. The respective polyphenol solution (5 mL total) was added dropwise into 25 mL of the PVA–Cin-Ch matrix under magnetic stirring while applying ultrasonication at 40% amplitude for 2.5 min to promote homogeneous molecular dispersion. Formulations loaded with curcumin (PVA–Cin-Ch–Cur) and quercetin (PVA–Cin-Ch–Quer), along with their unmodified chitosan counterparts (PVA–Ch–Cur and PVA–Ch–Quer), were prepared following the same procedure to evaluate individual loading and release kinetics. Ionic crosslinking was initiated by the controlled addition of 25 mL of TPP solution (0.5% w/v, pH 3) using a syringe pump while maintaining stirring at 600 rpm for 2 h. Following ionic crosslinking, the reaction dispersion was conditioned to induce reversible coacervative flocculation, allowing the hybrid nanoparticles to be efficiently sedimented at 9000 rpm (8880× g) for 20 min on a benchtop high-speed centrifuge without requiring high-energy ultracentrifugation. Due to the steric stabilization provided by the hydrated polyvinyl alcohol corona, the soft pellet was easily and fully redispersed into ultrapure water under mild agitation, restoring the pristine, unimodal submicron population (197–200 nm, PDI < 0.25) as confirmed by DLS analysis.

2.4. Physicochemical Characterization

Dynamic flash combustion elemental microanalysis (CHNO), isolated gravimetric reaction yield protocols, and orthogonal degree of substitution (DS) distribution across independent synthetic batches are detailed in Sections S1.1–S1.3 and S2.1–S2.3 in the Supplementary Information (Figure S1, Tables S1–S3).

2.5. UV–Visible and FTIR Spectroscopy

UV–Vis spectra (200–400 nm) of native chitosan, cinnamaldehyde, Cin-Ch, and the resulting nanoparticles were recorded using an Epoch II Microplate Reader (BioTek Instruments, Inc., Winooski, VT, USA) to confirm successful encapsulation and spectral shifts of curcumin and quercetin.

ATR–FTIR spectra (4000–500 cm^{-1}) were obtained using a Thermo Nicolet iS50 spectrometer (Thermo Fisher Scientific Inc., Madison, WI, USA). Spectra were collected for cinnamaldehyde, native chitosan, and synthesized Cin-Ch to verify chemical modification (Schiff base formation and subsequent reduction).

2.6. ^{1}H NMR Spectroscopy Analysis

The chemical structures and degree of substitution of native chitosan and cinnamyl-modified chitosan (Cin-Ch) were characterized using solution-state proton nuclear magnetic resonance (^{1}H NMR) spectroscopy on a Bruker AVANCE III 500 MHz spectrometer (Bruker, Billerica, MA, USA) operating at 500.13 MHz. Samples (10 mg) were dissolved in 1.0 mL of deuterated acidic solvent consisting of 1% (*v*/*v*) trifluoroacetic acid-d (CF_3COOD) in deuterium oxide (D_2O, 99.9 atom % D, Sigma-Aldrich, Darmstadt, Germany). The suspensions were stirred under ambient conditions for 6 h to achieve complete dissolution and subsequently transferred into standard 5 mm NMR tubes. Spectra were acquired at an elevated temperature of 70 °C (343 K) to attenuate solution viscosity and eliminate line-broadening artifacts caused by the hydrophobic self-association and π–π stacking of the aromatic cinnamyl residues. Acquisition parameters were configured as follows: a 90° pulse angle of 10.2 µs, a spectral width of 10,000 Hz, an acquisition time of 3.27 s, a relaxation delay (d1) of 2.0 s, and 64 accumulated scans. Chemical shifts (δ) are expressed in parts per million (ppm) calibrated against the residual solvent resonance signal (HOD/H_2O at δ = 4.79 ppm). The degree of cinnamyl substitution (DS_{NMR}%) on the chitosan backbone was determined quantitatively by comparing the integral area of the five aromatic protons of the cinnamyl group (δ = 7.25–7.50 ppm, 5H) with the integral area corresponding to the glucosamine ring protons (H–2 through H–6, δ = 3.10–4.10 ppm, 6H) according to Equation (1) [43,44]:

$$DS_{NMR}\% = \frac{I_{aromatic}/5}{I_{H2–H6}/6} \times 100 \quad (1)$$

2.7. X-Ray Photoelectron Spectroscopy (XPS) Analysis

Surface elemental composition and chemical bonding environments of native chitosan (CHI) and cinnamyl-modified chitosan (Cin-Ch) powders were analyzed using an ESCALAB 250Xi X-ray photoelectron spectrometer (Thermo Fisher Scientific, East Grinstead, UK) equipped with a monochromatic Al *Kα* X-ray source ($h\nu$ = 1486.6 eV) operating at 15 kV and 150 W. Powder samples were immobilized on sample stubs using conductive copper tape and degassed in the preparation chamber until an ultra-high vacuum base pressure ($<5 \times 10^{-9}$ mbar) was attained. Wide-scan survey spectra were acquired across an energy window of 0–1000 eV with a pass energy of 150 eV and an energy step size of 1.0 eV. High-resolution core-level spectra for C 1*s* (280–293 eV) and N 1*s* (394–406 eV) were recorded at a pass energy of 20 eV with a step size of 0.05 eV and 15 accumulated sweeps. Static charge compensation was achieved using an automated low-energy electron/ion flood gun, and binding energies were calibrated by referencing the adventitious aliphatic C 1*s* (C–C/C–H) peak to 284.8 eV. Peak deconvolution and curve fitting were performed using Thermo Avantage software (v5.99), applying non-linear Shirley background subtraction and mixed Gaussian–Lorentzian (GL 30) peak functions [45,46].

2.8. Particle Size, Zeta Potential, and Storage Stability

Dynamic light scattering and zeta potential (ζ) analyses were performed using a Zetasizer Nano ZS (Malvern Instruments, Great Malvern, UK) at 25 °C. Samples were diluted in deionized water and gently passed through 0.45 µm PTFE syringe filters immediately prior to measurement solely to eliminate dust particulates and macroscopic aggregates that could disrupt optical autocorrelation. The hydrodynamic diameter, polydispersity index (PDI), and zeta potential were recorded for each formulation in triplicate at 25 °C. To evaluate colloidal storage stability and rule out aggregation, aqueous dispersions of optimized PVA–Cin-Ch–Cur and PVA–Cin-Ch–Quer were stored at 4 °C protected from light, and their hydrodynamic diameter and PDI were recorded on days 0, 7, and 14.

2.9. Surface Wettability and Static Contact Angle Measurement

The modulation of intrinsic macromolecular surface polarity upon cinnamaldehyde functionalization was evaluated via static water contact angle measurements on solvent-cast planar films of the respective polymers (native chitosan and Cin-Ch), rather than compacted particulate powders, to eliminate roughness and porosity artifacts. Homogeneous polymer solutions (1.0% w/v in 1% v/v aqueous lactic acid) were cast onto clean, smooth Parafilm M substrates to ensure an inert, planar baseline and dried under ambient conditions. Deionized water droplets (5 µL) were deposited via an automated microsyringe onto the film surfaces at 25 °C. Contact angles were recorded within 5 s of sessile droplet stabilization across nine independent replicates ($n = 9$) on different surface locations, and results are expressed as mean ± standard deviation.

2.10. Encapsulation Efficiency and Loading Efficiency

Encapsulation and loading efficiencies were calculated based on the amount of unencapsulated curcumin and quercetin remaining in the supernatant after centrifugation. The concentrations of curcumin and quercetin were quantified using UV–Vis spectrophotometry at 429 nm and 372 nm, respectively, with pre-established calibration curves. Encapsulation Efficiency (EE%) and Loading Efficiency (LE%) were calculated as:

$$EE(\%) = \frac{m_i - m_f}{m_i} \times 100 \quad (2)$$

$$LE(\%) = \frac{m_e}{m_e + m_p} \times 100 \quad (3)$$

where m_i is the total mass of drug used, m_f is the mass of unencapsulated drug in the supernatant, and m_p is the mass of PVA–Cin-Ch used in the formulation.

2.11. Quantification of Free Amine Groups via TNBS Assay

The degree of primary amino group substitution (DS_{TNBS}, %) was quantified using the 2,4,6-trinitrobenzene sulfonic acid (TNBS) colorimetric assay adapted from established protocols [47]. Briefly, sample solutions (2.0 mg/mL) were reacted with 0.1% (w/v) TNBS in 0.1 M $NaHCO_3$ buffer (pH 8.5) and incubated in the dark at 40 °C for 2 h. After acidification with 1 M HCl to terminate the reaction, the optical density was measured at 344 nm against a native chitosan baseline on an Epoch II microplate spectrophotometer. The degree of substitution (DS_{TNBS}, %) was calculated according to Equation (3) [40]:

$$DS_{TNBS}(\%) = \left(1 - \frac{A_{Cin-Ch}}{A_{CHI}}\right) \times 100 \quad (4)$$

where A_{Cin-Ch} and A_{CHI} denote the blank-corrected absorbances of cinnamyl-modified chitosan and unmodified native chitosan, respectively. All determinations were executed across nine independent replicates ($n = 9$).

2.12. In Vitro Release Studies

To evaluate release kinetics, 10 mg of freeze-dried nanoparticles were dispersed in 50 mL of a hydroalcoholic medium (H_2O:EtOH = 3:2, v/v) and maintained at 37 °C under stirring (500 rpm). Samples (2 mL) were withdrawn at specific intervals, centrifuged, and analyzed by UV–Vis spectroscopy at 429 nm (CUR) and 372 nm (QC). Withdrawn volumes were replaced with equal amounts of fresh medium to maintain sink conditions. Cumulative release (R_t) was calculated as:

$$R_t(\%) = \frac{C_t V_t + \sum_{i=1}^{n-1} C_i V_i}{C_0 V_0} \times 100 \quad (5)$$

where C_t is the concentration at time t, V_t is the sample volume, and C_0V_0 is the total amount of loaded compound.

2.13. Antifungal Activity Assay

The antifungal efficacy of native chitosan, Cin-Ch, free curcumin, free quercetin, and polyphenol-loaded hybrid nanoparticles (PVA–Cin-Ch–Cur and PVA–Cin-Ch–Quer) was evaluated against *Aspergillus niger* and *Penicillium digitatum* using qualitative agar disc diffusion and standardized broth microdilution protocols. Fungal conidial suspensions were harvested from 7-day-old sporulating cultures in sterile saline with 0.05% (*v*/*v*) Tween 80 and adjusted using a densitometer (Biosan, Riga, Latvia).

For qualitative agar diffusion assays, DRBC agar plates were spread-inoculated with spore suspensions standardized to 2 McFarland (~1.0×10^6 CFU/mL) to achieve uniform microbial lawns. Sterile paper discs (6.0 mm diameter) impregnated with 50 µL of the test formulations (50–5000 ppm for free compounds; 0.5–50% *w*/*v* for nanoparticles dispersions) were placed on the inoculated plates and incubated at 30 °C for 7 days, after which the diameters of the growth suppression zones were recorded. These diffusion assays were used strictly for comparative topical screening and were not used to compute MIC values.

Quantitative Minimum Inhibitory Concentrations (MICs) were determined via broth microdilution in 96-well flat-bottom microplates according to CLSI M38-A2 guidelines. Conidial suspensions were standardized to 0.5 McFarland and diluted into YPD and SDA broths to yield a final well inoculum of approximately $1.0–5.0 \times 10^4$ CFU/mL. Serial two-fold dilutions of free agents and hybrid nanoparticles were incubated at 30 °C for 7 days. To prevent hyphal sedimentation and clumping artifacts associated with single-wavelength optical density readings, MIC was defined visually as the lowest concentration completely preventing discernible hyphal germination and growth compared to vehicle controls. Viability endpoints were verified metabolically using a resazurin dye reduction assay (0.02% *w*/*v*, read at λ_{ex} = 530 nm/λ_{em} = 590 nm), where the absence of blue-to-pink colorimetric transition confirmed complete hyphal inactivation.

3. Results and Discussion

3.1. FTIR Analysis of Cin-Ch

The covalent grafting of cinnamaldehyde onto the chitosan backbone via reductive amination was established by ATR-FTIR spectroscopy (Figure 1). The FTIR spectrum of unmodified chitosan exhibited characteristic polysaccharide absorption bands, including the broad envelope spanning 3600–3100 cm^{-1} [48,49] (O–H and primary N–H stretching), aliphatic C–H stretching at 2878 cm^{-1} [50,51], residual chitin Amide I (C=O stretching) at 1652 cm^{-1} [45,52], and the dominant Amide II primary amine deformation (–NH_2 bending) at 1590 cm^{-1} [43,45]. In the fingerprint region, the asymmetric glycosidic bridge (C–O–C) and skeletal pyranose ring vibrations were resolved at 1152, 1065, and 1025 cm^{-1} [53,54].

In the spectrum of the cinnamaldehyde precursor, the conjugated aldehydic carbonyl (C=O) stretch appeared as an intense, sharp band at 1678 cm^{-1} [55,56], complemented by the diagnostic aldehydic C–H Fermi doublet at 2815 and 2742 cm^{-1} [57,58], conjugated alkene (C=C) stretching at 1625 cm^{-1} [59,60], *trans*-alkene out-of-plane bending at 972 cm^{-1} [61] and monosubstituted benzene ring deformations at 748 and 688 cm^{-1} [54].

Following the reductive amination reaction, the FTIR spectrum of Cin-Ch demonstrated definitive spectral transitions confirming covalent modification and high chemical purity. The sharp aldehydic carbonyl peak at 1678 cm^{-1} [58,62] and the corresponding aldehydic Fermi doublet (2815/2742 cm^{-1}) [63] completely disappeared, ruling out the presence of unreacted or physically entrapped free cinnamaldehyde. Concurrently, the primary amine Amide II band (1590 cm^{-1}) decreased significantly, giving rise to an overlapping band at

1648 cm^{-1} and a distinct secondary amine aliphatic C–N stretching vibration at 1262 cm^{-1}, confirming the complete borohydride reduction of the intermediate Schiff base (–N=CH–) into a stable secondary amine bridge (–NH–CH_2–). The preservation of the conjugated *trans*-alkene spacer and phenyl ring was verified by the retention of the characteristic *trans*–alkene out-of-plane bending band at 968 cm^{-1} and monosubstituted aromatic C–H out-of-plane bands at 746 and 692 cm^{-1}. The preservation of the skeletal pyranose framework between 1150 and 1020 cm^{-1} [56] confirmed that the covalent modification proceeded without disrupting the polysaccharide backbone.

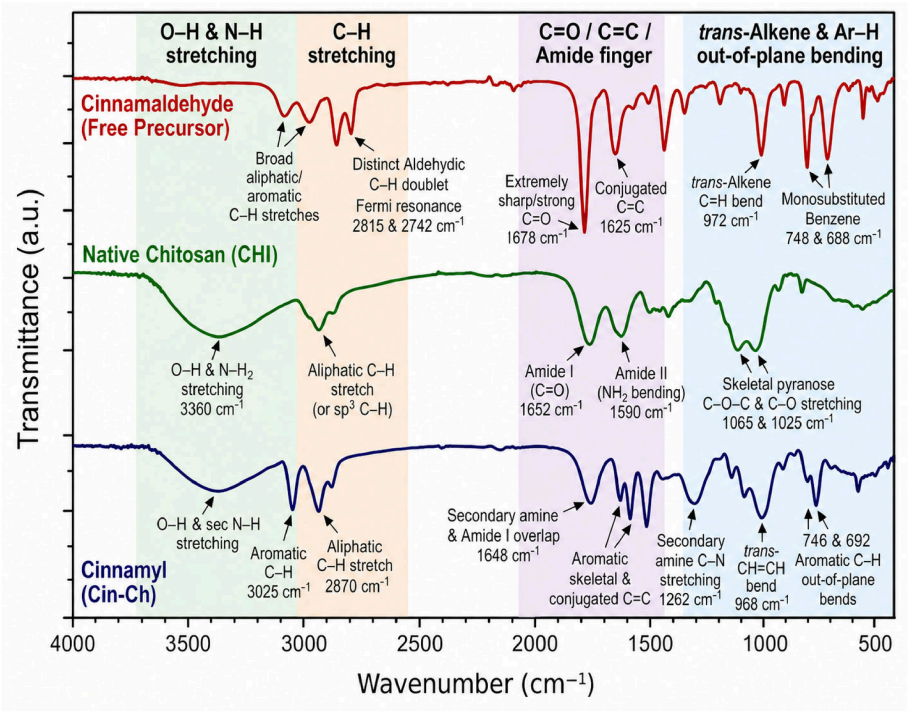


Figure 1. FTIR spectra of cinnamaldehyde, chitosan, and Cin-Ch.

3.2. Spectroscopic Structural Validation via ^{1}H NMR

The covalent functionalization of the chitosan backbone via reductive amination with cinnamaldehyde was corroborated by high-resolution ^{1}H NMR spectroscopy (Figure 2). In the spectrum of unmodified chitosan (Figure 2A), characteristic pyranose resonances are resolved, where the singlet at δ = 2.05 ppm corresponds to the methyl protons of residual *N*-acetylglucosamine units (–$NHCOCH_3$), the signal at δ = 3.10 ppm represents the H–2 proton of the glucosamine ring, and the broad envelope spanning δ = 3.50–4.10 ppm corresponds to the non-anomeric skeletal pyranose protons (H–3 through H–6). The anomeric proton (H–1) appears adjacent to the residual solvent peak (HOD) at δ = 4.60 ppm, verifying the integrity of the unfunctionalized polysaccharide framework [36].

Following reductive amination, the spectrum of cinnamyl chitosan (Figure 2B) displays distinct resonance signals that substantiate the installation of the hydrophobic phenylpropanoid moiety onto the polymer chains [34]. The appearance of a multiplet between δ = 7.25 and 7.50 ppm integrates to five protons, confirming the presence of the aromatic cinnamyl ring (–C_6H_5), while the retention of the conjugated alkene spacer is evidenced by two discrete olefinic resonances: a doublet at δ = 6.62 ppm with a vicinal coupling constant of J = 15.8 Hz, corresponding to the α-olefinic proton adjacent to the phenyl ring (–Ph–CH=CH–), and a multiplet at δ = 6.38 ppm that corresponds to the β-olefinic proton (=CH–CH_2–). Crucially, the magnitude of the coupling constant (J > 15 Hz) demon-

strates that the *trans* (*E*) stereochemistry of the cinnamyl precursor remained unperturbed throughout the coupling and reduction steps.

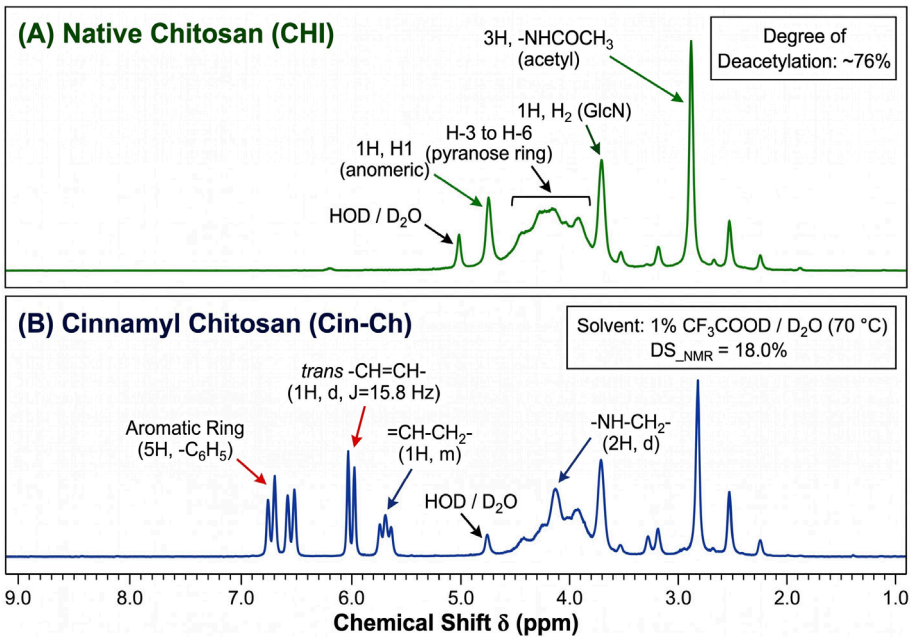


Figure 2. Comparative ^{1}H NMR spectra (500 MHz, 1% CF_3COOD/D_2O, 70 °C) of (**A**) native chitosan (CHI) and (**B**) cinnamyl-modified chitosan (Cin-Ch), demonstrating successful covalent functionalization, secondary amine formation (–NH–CH_2– at δ = 3.42 ppm), retention of *trans*-stereochemistry (J = 15.8 Hz at δ = 6.62 ppm), and a degree of substitution (DS_{NMR}) of 18.0%.

The complete reduction of the transient Schiff base imine intermediate (–N=CH–, typically located at δ≈8.2 ppm and absent here) into a stable secondary amine linkage is verified by the diagnostic doublet emerging at δ = 3.42 ppm (2H, d), which was assigned to the aliphatic methylene bridge (–NH–CH_2–CH=CH–*Ph*). Quantitative spectral integration comparing the cinnamyl aromatic envelope (δ = 7.25–7.50 ppm, 5H) to the skeletal pyranose protons (H–2 to H–6, δ = 3.10–4.10 ppm, 6H) establishes a degree of substitution (DS_{NMR}) of 18.0%. This quantitative finding exhibits stoichiometric convergence with both the primary amine consumption measured by the colorimetric TNBS assay (18.1% ± 0.3%) and the carbon-enrichment balance determined via elemental microanalysis (18.2%). The consistency across these orthogonal techniques confirms that cinnamyl moieties were grafted statistically and homogeneously along the glucosamine units without inducing excessive polymer rigidification or backbone scission [64,65].

The covalent modification, batch-to-batch reproducibility, and substitution distribution of Cin-Ch were further validated orthogonally by dynamic elemental microanalysis (CHNO) and gravimetric yield measurements across triplicate synthetic batches (Supplementary Information, Figure S1 and Tables S1–S3). Elemental analysis revealed a stoichiometric shift in the atomic C/N weight ratio from 5.16 ± 0.04 (native chitosan) to 6.85 ± 0.05 (Cin-Ch), establishing a calculated degree of substitution (DS_{EA}) of 18.2% (Table S1). This value demonstrates quantitative convergence with the ^{1}H NMR spectral integration (18.0%) and the colorimetric TNBS primary amine titration (18.1% ± 0.3%, CV = 1.33%), confirming a statistically uniform distribution of cinnamyl residues along the polysaccharide chains without localized block aggregation (Table S3). Furthermore, the mean isolated reaction yield of purified Cin-Ch powder was 78.4% ± 3.2% (Figure S1C and Table S2), confirming high synthetic recovery and minimal biopolymer mass loss during purification.

3.3. Surface Chemical Profiling via X-Ray Photoelectron Spectroscopy (XPS)

The surface chemical states and covalent bond modifications resulting from cinnamaldehyde grafting were verified by XPS analysis (Figure 3). The wide-scan survey spectra of unmodified chitosan and Cin-Ch (Figure 3A) exhibit the principal photoelectron lines corresponding to oxygen (O 1*s* at ~532.5 eV), nitrogen (N 1*s* at ~400.0 eV), and carbon (C 1*s* at ~285.0 eV). Following reductive amination, the relative intensity of the C 1*s* envelope increased noticeably in Cin-Ch, accompanied by a corresponding attenuation of the N 1*s* and O 1*s* signals. This surface carbon enrichment directly reflects the incorporation of the carbon-rich cinnamyl phenylpropanoid skeleton onto the outer atomic layers of the biopolymer particles [41,45,66].

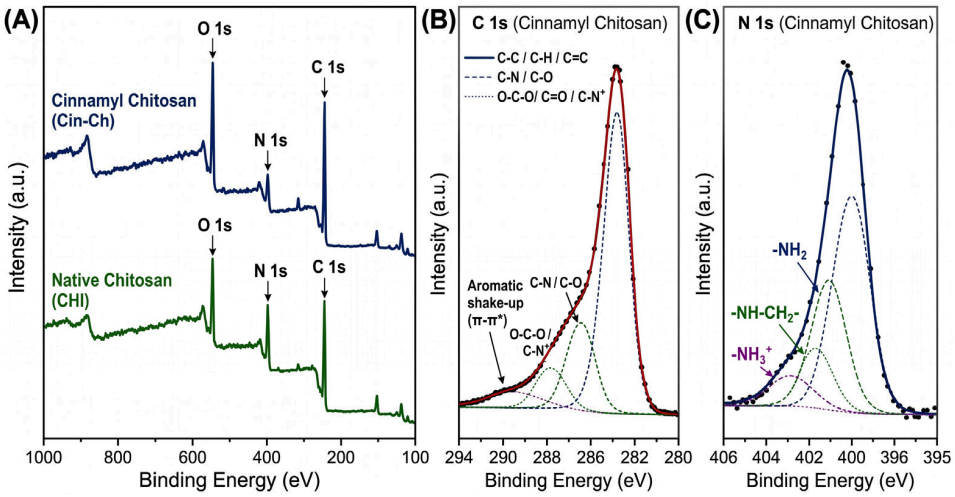


Figure 3. Surface chemical state characterization of unmodified chitosan (CHI) and cinnamyl-modified chitosan (Cin-Ch) via X-ray photoelectron spectroscopy (XPS): (**A**) wide-scan XPS survey spectra showing C 1*s*, N 1*s*, and O 1*s* core levels; (**B**) high-resolution deconvoluted C 1*s* core spectrum of Cin-Ch highlighting the aromatic $\pi \rightarrow \pi^*$ shake-up satellite feature at 291.2 eV; and (**C**) high-resolution deconvoluted N 1*s* core spectrum of Cin-Ch demonstrating the emergence of the secondary amine linkage (–NH–CH_2– at 399.4 eV) post-reduction.

High-resolution deconvolution of the C 1*s* core level of Cin-Ch (Figure 3B) resolves into five distinct chemical contributions: the major envelope at 284.8 eV (C–C/C = C) arising from both the conjugated aromatic cinnamyl ring and aliphatic carbons, the C–N bond at 285.8 eV, the pyranose ether/hydroxyl C–O carbons at 286.6 eV, and the residual acetamido carbonyl (O–C–O/C = O) at 288.2 eV. Significantly, a distinct shake-up satellite peak was identified at 291.2 eV. This characteristic satellite resonance corresponds to $\pi \rightarrow \pi^*$ electronic transitions within conjugated aromatic systems, providing direct surface spectroscopic confirmation of the intact benzene ring belonging to the grafted cinnamyl moiety [39].

The transformation of primary amine functionalities into secondary amine linkages was quantitatively corroborated by deconvoluting the N 1*s* narrow-scan spectrum of Cin-Ch (Figure 3C). The spectrum resolves into three sub-components: unmodified primary amine groups (–NH_2) at 400.1 eV, residual protonated amine species (–NH_3^+) at 401.8 eV, and a newly emerged peak centered at 399.4 eV. This lower binding energy peak at 399.4 eV is assigned to the neutral secondary aliphatic amine bridge (–NH–CH_2–), demonstrating the complete reduction of the intermediate Schiff base imine bonds (–N=CH–). Component area quantification indicates that secondary amines account for 52.4% of the total nitrogen envelope, demonstrating efficient functionalization of available amine sites. These surface-level findings correlate with the bulk ^{1}H NMR and TNBS determinations, verifying stable covalent conjugation without polymer degradation.

3.4. Determination of Free Amine Groups with TNBS Assay

The degree of primary amine substitution (DS%) was quantified by the 2,4,6-trinitrobenzene sulfonic acid (TNBS) assay, which selectively reacts with free amino groups to produce a chromogenic derivative detectable at 344 nm. Optical density (OD_{344}) values and corresponding statistical analyses are summarized in Table 1. A notable reduction in absorbance was observed for Cin-Ch compared to unmodified chitosan, indicating the consumption of amino groups during reductive amination.

Table 1. TNBS assay results.

Sample	Replicate Count	Mean OD_{344}	Std. Dev	CV (%)
CHI	9	2.227	0.028	1.27
Cin–Ch	9	1.824	0.024	1.33

Based on the experimental data, the degree of substitution was determined to be 18.1%, confirming partial modification of the polymer backbone while retaining sufficient free amine sites for further crosslinking and interaction within the PVA–Cin-Ch system [66,67].

Absorbance at 344 nm decreased significantly in the Cin-Ch samples compared to native chitosan, indicating the consumption of amino groups during the reductive amination process (Table 1). Based on the absorbance ratios, the degree of substitution was calculated as 18.1%, confirming partial modification of the chitosan backbone.

This level of substitution suggests that approximately one-fifth of the primary amino groups were successfully grafted with cinnamaldehyde residues. Such moderate substitution is consistent with literature values reported for N-substituted chitosan derivatives, where substitution levels between 15% and 25% are considered optimal for maintaining solubility and crosslinking capacity while imparting additional hydrophobic and antimicrobial characteristics [68,69]. Higher degrees of substitution can lead to excessive rigidity and reduced ionic reactivity, whereas very low substitution fails to provide sufficient functional enhancement.

Therefore, the observed 18.1% substitution indicates a balanced modification that preserves reactive amino sites necessary for TPP-mediated ionic crosslinking in nanoparticles formation, while introducing enough cinnamyl functionality to alter the chemical environment of the polymer. This controlled substitution is expected to play a key role in both encapsulation efficiency and antifungal performance, which are discussed in subsequent sections.

3.5. Contact Angle and Surface Wettability Analysis

The modulation of intrinsic polymer surface polarity following cinnamaldehyde modification was verified by sessile drop contact angle analysis on cast polymer films (Figure 4). The static water contact angle of native chitosan films was measured as 93.2° ± 2.1°, whereas that of Cin-Ch films increased significantly to 107.4° ± 2.4° ($p < 0.001$, $n = 9$). This marked 14.2° elevation in contact angle reflects the covalent grafting of hydrophobic phenylpropanoid moieties onto the hydrophilic glucosamine backbone, which lowers surface free energy and reduces polar water affinity. The uniform cast films on inert Parafilm substrates exhibited minimal surface roughness variations, ensuring that the wetting difference is strictly governed by chemical surface functionality rather than topography. These findings confirm the successful conversion of hydrophilic chitosan into a structurally hydrophobic polymer matrix, providing favorable hydrophobic microdomains essential for high-affinity encapsulation and retention of hydrophobic polyphenols (curcumin and quercetin) [70,71].

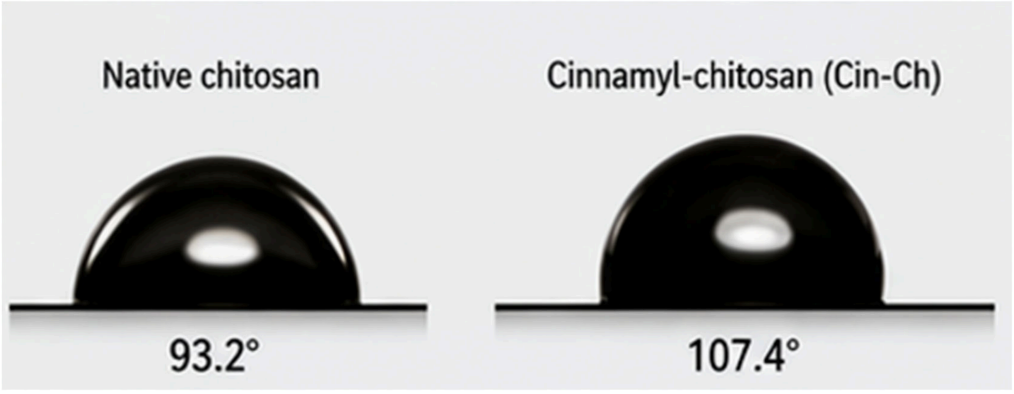


Figure 4. Static water contact angles of native chitosan (93.2° ± 2.1°) and cinnamyl chitosan (107.4° ± 2.4°) films cast on inert Parafilm substrates ($n = 9$).

3.6. Optimization of Nanoencapsulation

Encapsulation efficiency (EE%) and loading capacity (LC%) were optimized through a series of preliminary experiments in which chitosan–TPP ratios were kept constant while solvent type and surfactant concentration were systematically varied. Encapsulation efficiency was quantified by measuring the concentration of unencapsulated CUR and QC in the supernatants using their respective calibration curves (Figure 5), and the outcomes of all trials are summarized in Table 2.

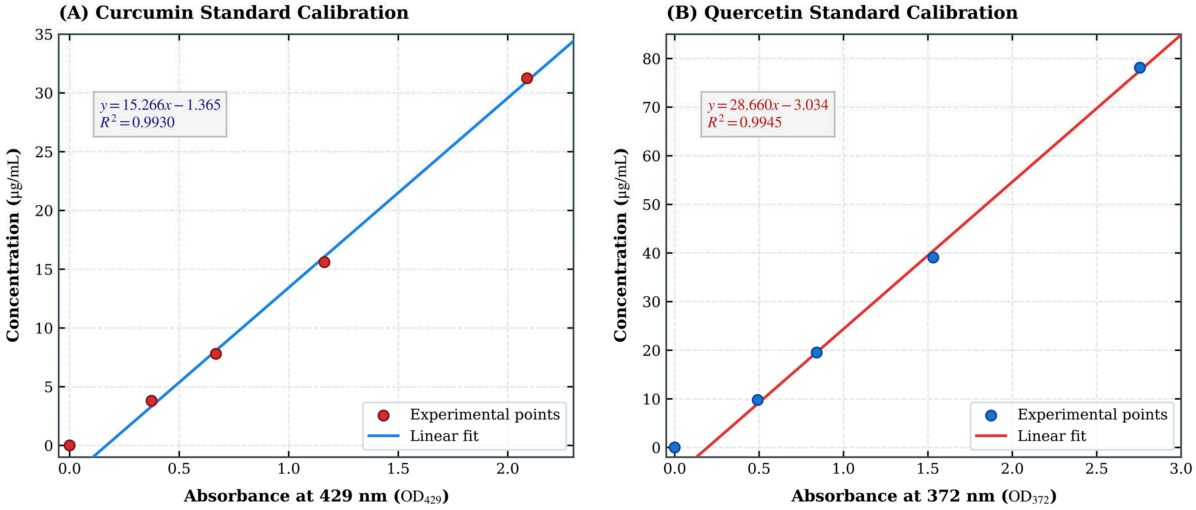


Figure 5. Standard spectrophotometric calibration curves of (**A**) curcumin at λ_{max} = 429 nm ($y = 15.266x - 1.365$, $R^2 = 0.9930$) and (**B**) quercetin at λ_{max} = 372 nm ($y = 28.660x - 3.034$, $R^2 = 0.9945$) in dimethyl sulfoxide (DMSO) across serial dilution ranges. Solid lines represent linear regression fits.

A clear solvent-dependent effect was observed. When ethanol was used to dissolve CUR and QC, encapsulation efficiencies remained below 60%, even in the presence of Tween 80. Ethanol's limited capacity to solubilize hydrophobic polyphenols resulted in premature precipitation and poor dispersion within the polymer matrix, ultimately restricting entrapment during ionic gelation. In contrast, the use of DMSO markedly improved encapsulation performance, increasing EE% to above 90% and exceeding 98% under optimized conditions. The enhanced solubility of CUR and QC in DMSO promoted more uniform miscibility with the chitosan-based matrix and minimized phase separation prior to crosslinking. These findings align with previous reports demonstrating the effectiveness of DMSO in dissolving hydrophobic phenolic compounds and facilitating homogeneous encapsulation [72,73].

Table 2. Nanoencapsulation trials and comparison.

Sample	Tween 80 (%)	Solvent	Active Ingredient (mg)	Encapsulation Efficiency (%)	Loading Capacity (%)
PVA–Ch–Cur v1	0	EtOH	20	53.4	—
PVA–Ch–Cur v2	1	EtOH	20	56.0	—
PVA–Ch–Cur v3	1	DMSO	100	83.7	25.9
PVA–Ch–Cur v4	0	DMSO	100	97.9	28.0
PVA–Ch–Cur v5	0	DMSO	250	99.9	43.1
PVA–Ch–Quer v1	0	EtOH	20	30.6	—
PVA–Ch–Quer v2	1	EtOH	20	31.0	—
PVA–Ch–Quer v3	1	DMSO	100	90.4	19.9
PVA–Ch–Quer v4	0	DMSO	100	91.0	30.0
PVA–Ch–Quer v5	0	DMSO	250	98.4	38.4
PVA–Cin-Ch–Cur	0	DMSO	250	99.99	64.8
PVA–Cin-Ch–Quer	0	DMSO	250	99.85	57.3

The influence of surfactant concentration was also investigated by varying Tween 80 from 0–1%. Although surfactants are commonly used to improve emulsification, Tween 80 showed no significant impact on EE% or LC%, indicating that the PVA–Cin-Ch matrix already provided sufficient interfacial stabilization for uniform droplet formation. The highest efficiencies were consistently achieved in Tween-free, DMSO-based systems, confirming that additional surfactants were unnecessary.

Based on these findings, the optimized encapsulation formulation was established as follows: 25 mL of 1% (w/v) chitosan or Cin-Ch in 2% lactic acid, 25 mL of 0.5% (w/v) TPP solution (pH 3), and 250 mg of CUR or QC dissolved in 5 mL DMSO.

Under these optimized conditions, encapsulation efficiencies exceeded 99%, while loading capacities reached approximately 43% for chitosan-based nanocolloidal particles and over 60% for Cin-Ch systems. The superior loading achieved with Cin-Ch is attributed to its increased hydrophobicity and the presence of aromatic cinnamyl moieties, which enhance molecular affinity and retention of polyphenolic compounds during the gelation process.

These results demonstrate that DMSO without surfactant provides the optimal environment for forming stable, high-loading PVA–Cin-Ch–Cur and PVA–Cin-Ch–Quer nanoparticles, balancing polymer compatibility, solubility, and entrapment efficiency. The observed improvement in encapsulation and loading efficiencies in the Cin-Ch formulations supports the hypothesis that the aromatic modification enhances hydrophobic interactions between the polymer and phenolic compounds [66,74,75]. The π–π stacking and van der Waals interactions between cinnamyl and polyphenolic rings likely contribute to more efficient entrapment with reducing leakage during gelation.

It should be noted that in all optimized formulations, PVA serves as an essential blending component (3:1 v/v) to provide physical stability and structural integrity to the crosslinked network. The superior loading capacities achieved in the PVA–Cin-Ch systems (64.8% for CUR and 57.3% for QC) compared to PVA–Ch counterparts confirm the crucial role of cinnamyl hydrophobic domains in retaining polyphenolic bioactives during ionic crosslinking.

3.7. In Vitro Controlled Release Kinetics of Polyphenol-Loaded Formulations

The cumulative in vitro release profiles of curcumin and quercetin from native chitosan (PVA–Ch) and cinnamyl-modified chitosan (PVA–Cin-Ch) nanoparticles were monitored

over 24 h under sink conditions, as shown in Figures 6A and 6B, respectively. To preclude UV-Vis spectrophotometric cross-interference between the characteristic absorption bands of curcumin (λ = 429 nm) and quercetin (λ = 372 nm), each polyphenol was formulated and quantified individually across identical carrier architectures.

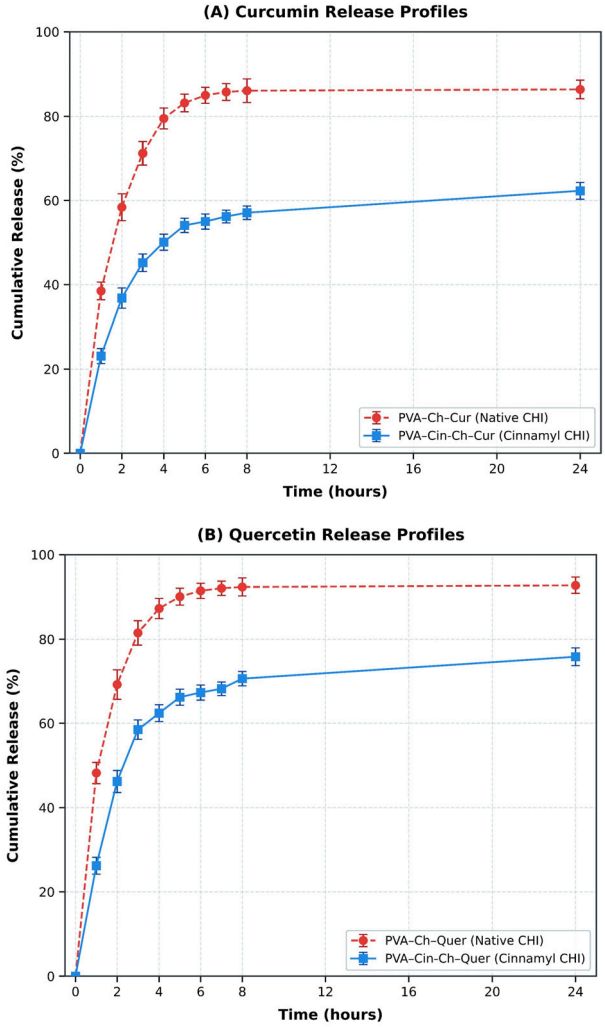


Figure 6. Comparative in vitro cumulative release kinetics of encapsulated polyphenols from native chitosan nanoparticles (PVA–Ch–Cur and PVA–Ch–Quer) and cinnamyl-functionalized hybrid nanoparticles (PVA–Cin-Ch–Cur and PVA–Cin-Ch–Quer) in hydroalcoholic buffer (H_2O:EtOH = 3:2, *v*/*v*, 37 °C, pH 7.4) over a 24-h incubation period: (**A**) curcumin release profiles and (**B**) quercetin release profiles. Data points represent the mean ± standard deviation of triplicate independent determinations (n = 3).

As illustrated in Figure 6A, the release kinetics of curcumin displayed substantial divergence between the unmodified and functionalized matrices. The unmodified native chitosan formulation (PVA–Ch–Cur) exhibited a rapid, pronounced burst release phase, discharging 38.5% ± 2.1% of the loaded curcumin within the first hour and 58.4% ± 3.2% by 2 h. This initial rapid diffusion progressively decelerated between 4 and 6 h, approaching a cumulative plateau of 86.1% ± 2.8% at 8 h and reaching 86.4% ± 2.2% at 24 h. Conversely, the cinnamyl-modified hybrid system (PVA–Cin-Ch–Cur) significantly mitigated the initial burst effect, releasing only 23.1% ± 1.8% at 1 h and 36.8% ± 2.4% at 2 h. Following this attenuated initial phase, the release proceeded through a sustained diffusion-governed regime (50.1% ± 1.9% at 4 h and 54.1% ± 1.7% at 5 h), ultimately stabilizing at an asymptotic plateau of 62.3% ± 2.0% at 24 h [76–78].

The corresponding release profiles of quercetin, depicted in Figure 6B, revealed an analogous structural dependency accompanied by systematically higher mass transfer rates. Unmodified nanoparticles (PVA–Ch–Quer) underwent extensive, rapid diffusion, expelling 48.2% ± 2.5% and 69.2% ± 3.5% of entrapped quercetin within 1 and 2 h, respectively. By 4 h, cumulative release reached 87.3% ± 2.4%, culminating in near-exhaustive release of 92.4% ± 2.1% at 8 h and 92.8% ± 1.9% after 24 h. In contrast, the incorporation of cinnamyl moieties in PVA–Cin-Ch–Quer successfully controlled the transport rate. Quercetin release was restricted to 26.2% ± 2.0% at 1 h and 46.2% ± 2.6% at 2 h, followed by a gradual release trajectory that reached 62.4% ± 2.0% at 4 h, 70.6% ± 1.7% at 8 h, and equilibrated at 75.8% ± 2.1% over the complete 24-h monitoring window [79,80].

Comparative analysis across both Figure 6A,B reveals the fundamental role of carrier chemistry and penetrant polarity in dictating release mechanisms. In unmodified PVA–Ch nanoparticles, the pronounced burst and high cumulative release (>86–92%) are governed by rapid aqueous swelling of the hydrophilic polysaccharide backbone, chain relaxation, and subsequent unhindered Fickian desorption of active agents localized near the submicron particle boundaries. In stark contrast, covalent grafting of cinnamyl residues in the PVA–Cin-Ch matrix establishes a dual-action diffusion barrier: the elevated matrix hydrophobicity restricts solvent wicking, while the exposed phenyl rings participate in strong non-covalent π–π stacking and hydrophobic interactions with the aromatic polycyclic cores of both polyphenols. Furthermore, the comparatively slower release rate and lower 24-h plateau of curcumin relative to quercetin across both systems reflect its higher lipophilicity ($\log P \approx 3.2$ vs. 1.8), which promotes stronger thermodynamic partitioning and steric retention within the hydrophobic microdomains of the crosslinked network.

3.8. Particle Size and Zeta Potential Analysis

Dynamic light scattering measurements were performed at 25 °C to evaluate the particle size distribution and surface charge of the prepared hybrid nanoparticles (Figure 7). PVA–chitosan nanoparticles exhibited mean hydrodynamic diameters of 204 nm (PDI = 0.337) for PVA–Ch–Cur and 182.1 nm (PDI = 0.276) for PVA–Ch–Quer. PVA–Cin-Ch nanoparticles displayed slightly smaller and highly uniform particle sizes, with 200.2 nm (PDI = 0.240) for PVA–Cin-Ch–Cur and 197.3 nm (PDI = 0.250) for PVA–Cin-Ch–Quer systems. All formulations exhibited narrow size distributions (PDI < 0.35), indicating good colloidal homogeneity and stability. The minor decrease in average particle size and PDI upon cinnamyl modification may be attributed to enhanced chain rigidity and reduced hydrogen bonding density of the modified chitosan, leading to tighter molecular packing during ionic gelation. The introduction of aromatic cinnamyl groups likely restricted polymer chain mobility, promoting the formation of smaller and more compact nanocolloidal particles. Although the formulations were initially conceived within a nanoencapsulation framework, DLS analyses revealed that the hydrodynamic diameters of both PVA–Ch and PVA–Cin-Ch systems consistently fell within the submicron range (182–204 nm) with low polydispersity indices (PDI < 0.35), confirming the formation of stable hybrid nanoparticles rather than micrometric aggregates or microparticles. The minimal resistance observed during sample clarification through 0.45 μm filters further corroborates that the vast majority of the synthesized colloidal population were well below 300 nm, ruling out significant particle exclusion by filtration [81,82].

Zeta potential measurements revealed a clear reduction in surface charge following both TPP crosslinking and cinnamyl modification. The ζ-potentials of the chitosan-based nanoparticles were +18.1 mV for Ch–Cur and +16.4 mV for Ch–Quer, whereas those of the Cin-Ch-based formulations were reduced to +9.25 mV and +8.76 mV, respectively. This decrease can be explained by the consumption of primary amine groups, responsible for

the cationic nature of chitosan, through ionic interactions with tripolyphosphate anions and covalent bonding with cinnamaldehyde via reductive amination [83,84].

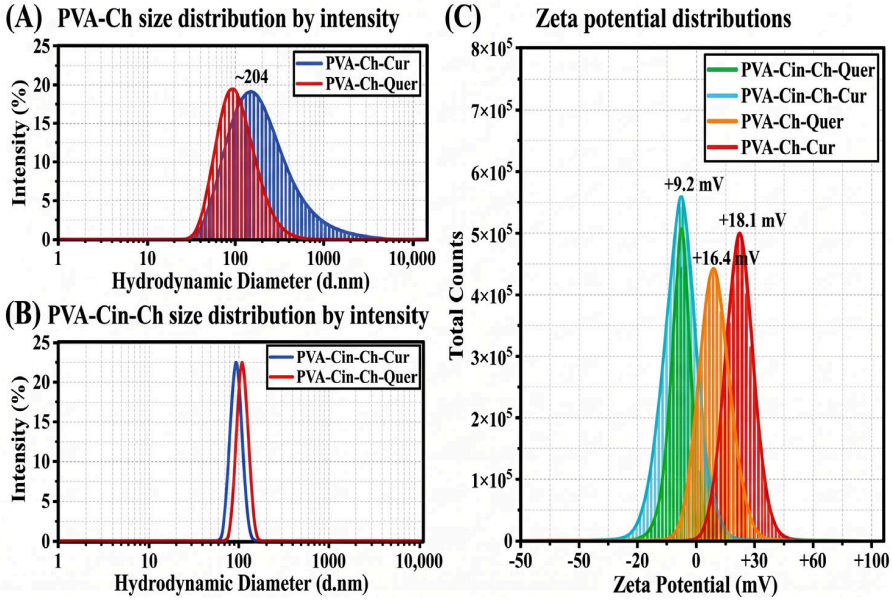


Figure 7. Hydrodynamic size and surface charge characterization of hybrid nanoparticles via dynamic light scattering (DLS) and electrophoretic light scattering at 25 °C: (**A**) number-weighted hydrodynamic diameter distributions of unmodified chitosan nanoparticles (PVA–Ch–Cur and PVA–Ch–Quer); (**B**) number-weighted size distributions of cinnamyl-functionalized nanoparticles (PVA–Cin-Ch–Cur and PVA–Cin-Ch–Quer); and (**C**) apparent zeta potential (ζ) distribution profiles illustrating the modulation of surface charge following covalent cinnamylation and ionic crosslinking.

Although the ζ-potentials of Cin-Ch nanocolloidal particles were below the typically reported +30 mV threshold for high electrostatic stability, no aggregation was observed during preparation or storage. This stability is primarily governed by steric stabilization provided by the extended, hydrated PVA polymer chains at the interface and the bulky cinnamyl groups, which prevent close inter-particle approach and compensate for the attenuated electrostatic repulsion. To verify this experimentally, the colloidal storage stability of the optimized dispersions was monitored over 14 days at 4 °C. Dynamic light scattering measurements revealed minimal size variations: PVA–Cin-Ch–Cur shifted marginally from 200.2 ± 3.1 nm (PDI = 0.240) on day 0 to 206.5 ± 4.2 nm (PDI = 0.248) on day 14, while PVA–Cin-Ch–Quer changed from 197.3 ± 2.8 nm (PDI = 0.250) to 203.8 ± 3.7 nm (PDI = 0.256). The absence of macroscopic sedimentation or significant PDI broadening confirms that steric stabilization provides robust dispersion stability over extended storage periods.

3.9. Antifungal Activity Assays

To decouple the relative contributions of the polymer backbone, the cinnamyl modifier, and nanoencapsulation, the antifungal activities of all eight experimental groups—free polyphenols (CUR and QC), unmodified chitosan (CHI), cinnamyl chitosan (Cin-Ch), and the respective nanoparticle formulations (PVA–Ch–Cur, PVA–Ch–Quer, PVA–Cin-Ch–Cur, and PVA–Cin-Ch–Quer)—were systematically evaluated against *P. digitatum* and *A. niger* (Table 3, Figure 8).

Native chitosan exhibited negligible inhibitory action (MIC > 2500 ppm), displaying only marginal sporulation delay against *P. digitatum* due to limited protonated amine interactions at near-neutral pH. In sharp contrast, cinnamyl-functionalized chitosan (Cin-Ch) demonstrated robust intrinsic antifungal activity, exhibiting MIC values of 250 ppm

against *P. digitatum* and 750 ppm against *A. niger*. This 3- to 10-fold enhancement stems from the grafted lipophilic cinnamyl groups, which act in concert with residual cationic amines to insert into and destabilize fungal ergosterol-rich lipid bilayers [85–87].

Table 3. Comprehensive Minimum Inhibitory Concentration (MIC, ppm) against *P. digitatum* and *A. niger*.

Sample Group	Form/Classification	MIC *P. digitatum* (ppm)	MIC *A. niger* (ppm)	Primary Inhibitory Mechanism
Native CHI	Unmodified Polysaccharide	>2500 (No complete kill)	>2500 (Inactive)	Weak surface polycationic interaction
Cin-Ch	Functionalized Polymer	250	750	Cationic binding + lipophilic membrane insertion
Free CUR	Free Polyphenol	1666	2500	Poor aqueous dispersion & slow passive influx
Free QC	Free Polyphenol	1666	2500	Rapid oxidative decay & limited cell penetration
PVA–Ch–Cur	Unmodified NPs (Cur)	500	833	Colloidal solubilization; moderate release
PVA–Ch–Quer	Unmodified NPs (Quer)	416	625	Enhanced bio-availability; moderate release
PVA–Cin-Ch–Cur	Modified Hybrid NPs (Cur)	62.5	125	Synergistic membrane disruption + sustained release
PVA–Cin-Ch–Quer	Modified Hybrid NPs (Quer)	46.8	93.7	Synergistic rapid initial burst + membrane damage

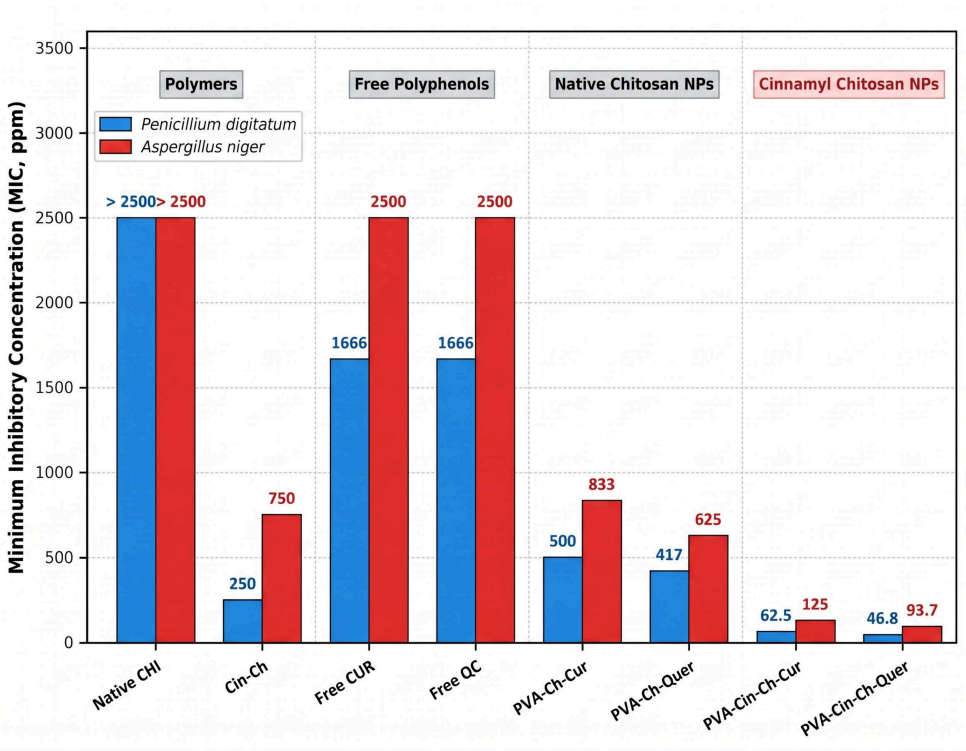


Figure 8. Comparative Minimum Inhibitory Concentration (MIC, ppm) of raw polymers (native CHI and Cin-Ch), free polyphenols (CUR and QC), unmodified chitosan nanoparticles (PVA–Ch–Cur and PVA–Ch–Quer), and cinnamyl-functionalized hybrid nanoparticles (PVA–Cin-Ch–Cur and PVA–Cin-Ch–Quer) against *Penicillium digitatum* and *Aspergillus niger*. All determinations were established via broth microdilution corroborated by resazurin metabolic activity profiling. Dashed vertical lines delineate polymer controls, free bioactives, native chitosan nanoformulations, and cinnamyl-modified hybrid systems.

Free CUR and QC displayed modest antifungal efficacy (MIC = 1666–2500 ppm), constrained primarily by poor aqueous solubility, self-aggregation, and rapid degradative precipitation in aqueous media. Encapsulation into unmodified chitosan nanoparticles (PVA–Ch–Cur and PVA–Ch–Quer) substantially improved performance (MIC = 416–833 ppm) by providing colloidal solubilization and preventing macro-aggregation [82,88].

The greatest antifungal potency was achieved by the cinnamyl-functionalized hybrid nanoparticles (PVA–Cin-Ch–Cur and PVA–Cin-Ch–Quer), which suppressed *P. digitatum* growth at 62.5 and 46.8 ppm, and *A. niger* at 125 and 93.7 ppm, respectively. This remarkable enhancement demonstrates a dual-action synergistic mechanism: the Cin-Ch outer network primes fungal envelope permeability via hydrophobic-electrostatic insertion, while the sustained biphasic release of the encapsulated polyphenols delivers high localized intracellular concentrations, triggering fatal oxidative and metabolic disruption.

4. Conclusions

In this study, a cinnamyl-functionalized chitosan (Cin-Ch) derivative was successfully synthesized via a two-step reductive amination protocol with an average isolated gravimetric reaction yield of 78.4% ± 3.2%. Multi-technique orthogonal characterization validated a precise and statistically uniform degree of substitution (DS ≈ 18%), demonstrated by the stoichiometric convergence among dynamic elemental microanalysis (DS_{EA} = 18.2%, atomic C/N weight ratio shift from 5.16 ± 0.04 to 6.85 ± 0.05), solution-state ^{1}H NMR spectroscopy (DS_{NMR} = 18.0%, trans-stereochemistry J = 15.8 Hz), and colorimetric primary amine titration via the TNBS assay (DS_{TNBS} = 18.1% ± 0.3%, CV = 1.33%). Covalent cinnamylation substantially lowered macromolecular surface energy, shifting the static water contact angle from 93.2° ± 2.1° to 107.4° ± 2.4° ($p < 0.001$) on planar films, while high-resolution XPS deconvolution verified the preservation of intact aromatic rings via a distinct $\pi \rightarrow \pi^*$ shake-up satellite at 291.2 eV and the formation of a stable secondary aliphatic amine linkage (–NH–CH_2– at 399.4 eV, constituting 52.4% of the total N 1s envelope).

Under optimized surfactant-free ionic gelation conditions, the formulated PVA–Cin-Ch hybrid nanocomposite platform achieved encapsulation efficiencies exceeding 99.8% (99.99% for curcumin and 99.85% for quercetin) with superior loading capacities of 64.8% and 57.3%, respectively. Dynamic light scattering established the formation of reproducible submicron colloids with unimodal distributions: 200.2 nm (PDI = 0.240) for PVA–Cin-Ch–Cur and 197.3 nm (PDI = 0.250) for PVA–Cin-Ch–Quer, which exhibited robust colloidal storage stability at 4 °C over 14 days without secondary aggregation or phase separation. The modulated surface charge (ζ = +9.25 mV and +8.76 mV) was physically compensated by the hydrated steric corona of polyvinyl alcohol chains, enabling complete aqueous redispersion following moderate-speed centrifugation (9000 rpm/8880× *g*).

Comparative in vitro release profiling over 24 h revealed that cinnamyl grafting effectively transformed the leaky, rapid burst release observed in unmodified chitosan nanoparticles (>86–92% release within 8 h) into a controlled, sustained biphasic diffusion regime, reaching 62.3% ± 2.0% for curcumin and 75.8% ± 2.1% for quercetin at 24 h. Broth microdilution assays corroborated by resazurin metabolic profiling confirmed potent synergistic antifungal efficacy: PVA–Cin-Ch–Cur and PVA–Cin-Ch–Quer suppressed fungal germination at Minimum Inhibitory Concentrations (MICs) of 62.5 ppm and 46.8 ppm against *Penicillium digitatum*, and 125 ppm and 93.7 ppm against *Aspergillus niger*, markedly outperforming free polyphenols (MIC = 1666–2500 ppm), unmodified native chitosan (MIC > 2500 ppm), and unmodified chitosan nanoparticles (MIC = 416–833 ppm). In conclusion, the ionically crosslinked PVA–Cin-Ch hybrid nanocarrier provides a chemically defined, scalable, and highly reproducible delivery vehicle for high-affinity payload retention, colloidal uniformity, and sustained bioactivity of hydrophobic polyphenolic antimicrobials.

Supplementary Materials: The following supporting information can be downloaded at: https://www.mdpi.com/article/10.3390/polym18222878/s1, Table S1: Elemental microanalysis (CHNO), atomic C/N mass ratios, and comparative degree of substitution (DS) of unmodified and cinnamyl-modified chitosan; Table S2: Isolated gravimetric reaction yield across three independent synthesis batches of cinnamyl chitosan (Cin-Ch); Table S3: Orthogonal cross-validation of degree of substitution (DS) across distinct analytical techniques; Figure S1: Quantitative elemental microanalysis and synthesis yield validation of cinnamyl-modified chitosan (Cin-Ch): (A) mass fractions (wt.%) of carbon, hydrogen, and nitrogen in native chitosan (CHI) and cinnamyl chitosan (Cin-Ch); (B) atomic C/N weight ratios with orthogonal convergence of the degree of substitution (DS) determined via elemental analysis (DS_EA = 18.2%), ^{1}H NMR spectroscopy (DS_NMR = 18.0%), and TNBS colorimetric titration (DS_TNBS = 18.1 ± 0.3%); (C) gravimetric isolated reaction yields across three independent consecutive batches with an average yield of 78.4 ± 3.2%. Refs. [40,66,82,88–94] are cited in the Supplementary Materials File.

Author Contributions: E.K.: Methodology, Resources, Formal Analysis, Data Curation, Validation, Writing—Original Draft; Writing—Review and Editing, O.T.: Methodology, Resources, Formal Analysis, Data Curation, Validation, Writing—Original Draft; Writing—Review and Editing, D.T.T.: Methodology, Resources, Formal Analysis, Data Curation, Validation, Writing—Original Draft; Writing—Review and Editing. A.A.K.: Methodology, Resources, Formal Analysis, Data Curation, Validation, Writing—Original Draft; Writing—Review and Editing. A.C.Ö.: Methodology, Resources, Formal Analysis, Data Curation, Validation, Writing—Original Draft; Writing—Review and Editing, F.C.: Methodology, Resources, Formal Analysis, Data Curation, Validation, Writing—Original Draft; Writing—Review and Editing. All authors have read and agreed to the published version of the manuscript.

Funding: The APC was funded by Istanbul Atlas University.

Institutional Review Board Statement: Not applicable.

Data Availability Statement: The original contributions presented in this study are included in the article. Further inquiries can be directed to the corresponding author.

Acknowledgments: While preparing this article, the authors used the ChatGPT (OpenAI, 2026) program for language editing. The results were plotted using the statistical software Origin 2022 and GraphPad Prism 9 based on the raw data from the original research. References were verified using the Mendeley program. The authors are solely responsible for the scientific interpretation and the final text of the article.

Conflicts of Interest: The authors declare no conflicts of interest.

References

1. Devecioglu, D.; Turker, M.; Karbancioglu-Guler, F. Antifungal Activities of Different Essential Oils and Their Electrospun Nanofibers against Aspergillus and Penicillium Species Isolated from Bread. *ACS Omega* **2022**, *7*, 37943–37953. [CrossRef]
2. Abad, A.V.; Manzanares, P.; Marcos, J.F.; Martínez-Culebras, P.V. The Penicillium digitatum antifungal protein PdAfpB shows high activity against mycobiota involved in sliced bread spoilage. *Food Microbiol.* **2023**, *109*, 104142. [CrossRef]
3. Beugelink, J.W.; Sweep, E.; Janssen, B.J.C.; Snijder, J.; Pronker, M.F. Structural Basis for Recognition of the FLAG-tag by Anti-FLAG M2. *J. Mol. Biol.* **2024**, *436*, 168649. [CrossRef]
4. Borgatta, M.; Breider, F. Inhalation of Microplastics—A Toxicological Complexity. *Toxics* **2024**, *12*, 358. [CrossRef]
5. Karahaliloğlu, Z.; Hazer, B. Curcumin- and quercetin-functionalized polypropylene membranes as active food packaging material. *J. Food Sci.* **2024**, *89*, 6575–6589. [CrossRef]
6. Koo, S.R.; Kim, J.T.; Chathuranga, K.; Lee, J.S.; Yoon, Y.I.; Park, W.H. PH-sensitive poly(vinyl alcohol)/quercetin/curcumin nanofiber membrane for food freshness monitoring. *Food Chem.* **2026**, *510*, 148613. [CrossRef]
7. Li, Y.; Shi, R.; Xu, Z.; Huang, T.; Wang, S.; Sang, Y.; Neves, M.A.; Yu, W.; Wang, X. Nanoparticles for Synergistic Delivery of Curcumin and Quercetin Based on Zein and Sodium Caseinate: Preparation, Characterization, and Intestinal Absorption. *Foods* **2026**, *15*, 225. [CrossRef]
8. Daglia, M. Polyphenols as antimicrobial agents. *Curr. Opin. Biotechnol.* **2012**, *23*, 174–181. [CrossRef]

9. Cenobio-Galindo, A.d.J.; Hernández-Fuentes, A.D.; González-Lemus, U.; Zaldívar-Ortega, A.K.; González-Montiel, L.; Madariaga-Navarrete, A.; Hernández-Soto, I. Biofungicides Based on Plant Extracts: On the Road to Organic Farming. *Int. J. Mol. Sci.* **2024**, *25*, 6879. [CrossRef]
10. Sellamuthu, G.; Chakraborty, A.; Vetukuri, R.R.; Sarath, S.; Roy, A. RNAi-biofungicides: A quantum leap for tree fungal pathogen management. *Crit. Rev. Biotechnol.* **2025**, *45*, 1131–1158. [CrossRef]
11. Yang, F.; Chen, C.; Ni, D.; Yang, Y.; Tian, J.; Li, Y.; Chen, S.; Ye, X.; Wang, L. Effects of Fermentation on Bioactivity and the Composition of Polyphenols Contained in Polyphenol-Rich Foods: A Review. *Foods* **2023**, *12*, 3315. [CrossRef]
12. Gürbüz, B.; Ciftci, F.; Özarslan, A.C.; Akyuz Yilmaz, B. MXene-modified PMMA/chitosan composite e-skin scaffold: Bioelectronic and antibacterial assessment. *Int. J. Biol. Macromol.* **2025**, *319*, 145388. [CrossRef]
13. Ciftci, F. Release kinetics modelling and in vivo-vitro, shelf-life study of resveratrol added composite transdermal scaffolds. *Int. J. Biol. Macromol.* **2023**, *235*, 123769. [CrossRef]
14. Dias, A.M.; Cabrera, M.P.d.S.; Lima, A.M.F.; Taboga, S.R.; Vilamaior, P.S.L.; Tiera, M.J.; Tiera, V.A.d.O. Insights on the antifungal activity of amphiphilic derivatives of diethylaminoethyl chitosan against Aspergillus flavus. *Carbohydr. Polym.* **2018**, *196*, 433–444. [CrossRef]
15. Gabriel, J.D.S.; Tiera, M.J.; Tiera, V.A.D.O. Synthesis, Characterization, and Antifungal Activities of Amphiphilic Derivatives of Diethylaminoethyl Chitosan against Aspergillus flavus. *J. Agric. Food Chem.* **2015**, *63*, 5725–5731. [CrossRef]
16. de Oliveira Pedro, R.; Takaki, M.; Gorayeb, T.C.C.; Del Bianchi, V.L.; Thomeo, J.C.; Tiera, M.J.; Tiera, V.A.d.O. Synthesis, characterization and antifungal activity of quaternary derivatives of chitosan on Aspergillus flavus. *Microbiol. Res.* **2013**, *168*, 50–55. [CrossRef]
17. de Carvalho, S.Y.B.; Almeida, R.R.; Pinto, N.A.R.; de Mayrinck, C.; Vieira, S.S.; Haddad, J.F.; Leitão, A.A.; Guimarães, L.G.d.L. Encapsulation of essential oils using cinnamic acid grafted chitosan nanogel: Preparation, characterization and antifungal activity. *Int. J. Biol. Macromol.* **2021**, *166*, 902–912. [CrossRef]
18. Beyki, M.; Zhaveh, S.; Khalili, S.T.; Rahmani-Cherati, T.; Abollahi, A.; Bayat, M.; Tabatabaei, M.; Mohsenifar, A. Encapsulation of Mentha piperita essential oils in chitosan-cinnamic acid nanogel with enhanced antimicrobial activity against Aspergillus flavus. *Ind. Crops Prod.* **2014**, *54*, 310–319. [CrossRef]
19. Badawy, M.E.I.; Rabea, E.I. Synthesis and structure-activity relationship of N-(cinnamyl) chitosan analogs as antimicrobial agents. *Int. J. Biol. Macromol.* **2013**, *57*, 185–192. [CrossRef]
20. Sahariah, P.; Másson, M. Antimicrobial Chitosan and Chitosan Derivatives: A Review of the Structure-Activity Relationship. *Biomacromolecules* **2017**, *18*, 3846–3868. [CrossRef]
21. Alamri, A.A.; Borik, R.M.A.; El-Wahab, A.H.F.A.; Mohamed, H.M.; Ismail, K.S.; El-Aassar, M.R.; Al-Dies, A.-A.M.; El-Agrody, A.M. Synthesis of Schiff bases based on Chitosan, thermal stability and evaluation of antimicrobial and antitumor activities. *Sci. Rep.* **2025**, *15*, 892. [CrossRef]
22. Gasmi, H.; Siepmann, F.; Hamoudi, M.; Danede, F.; Verin, J.; Willart, J.-F.; Siepmann, J. Towards a better understanding of the different release phases from PLGA microparticles: Dexamethasone-loaded systems. *Int. J. Pharm.* **2016**, *514*, 189–199. [CrossRef]
23. Triantafyllopoulou, E.; Forys, A.; Perinelli, D.R.; Balafouti, A.; Karayianni, M.; Trzebicka, B.; Bonacucina, G.; Valsami, G.; Pippa, N.; Pispas, S. Deciphering the Lipid-Random Copolymer Interactions and Encoding Their Properties to Design a Hybrid System. *Langmuir* **2024**, *40*, 11936–11946. [CrossRef]
24. Müller, W.A.; Beales, P.A.; Muniz, A.R.; Jeuken, L.J.C. Unraveling the Phase Behavior, Mechanical Stability, and Protein Reconstitution Properties of Polymer-Lipid Hybrid Vesicles. *Biomacromolecules* **2023**, *24*, 4156–4169. [CrossRef]
25. Joye, I.J.; McClements, D.J. Biopolymer-based nanoparticles and microparticles: Fabrication, characterization, and application. *Curr. Opin. Colloid Interface Sci.* **2014**, *19*, 417–427. [CrossRef]
26. Pastrana-Alta, R.Y.; Huarote-Garcia, E.; Egusquiza-Huamani, M.A.; Baena-Moncada, A.M. Antimicrobial activity of chitosan, alginate, pectin, and cellulose-based biopolymer composites with silver, copper oxide, and zinc oxide nanoparticles. *RSC Adv.* **2025**, *15*, 35807–35843. [CrossRef]
27. Panagiotou, T.; Fisher, R.J. Producing micron- And nano- size formulations for functional foods applications. *Funct. Foods Health Dis.* **2013**, *3*, 274–289. [CrossRef]
28. Verma, K.; Tarafdar, A.; Kumar, D.; Sari, T.; Badgujar, P.C.; Pareek, S.; Assadpour, E.; Jafari, S.M. Microfluidization based nano/sub-micron curcumin formulations for food and nutraceuticals: Physico-functional characteristics and safety aspects. *Food Chem.* **2025**, *485*, 144402. [CrossRef]
29. Kadriadi, E.A. A novel active packaging film based on polyvinyl alcohol/bajakah tampala (Spatholobus littoralis hassk) extract: Enhancing mechanical, UV protection, thermal stability, antimicrobial, and barrier properties. *Food Biosci.* **2025**, *68*, 106500. [CrossRef]
30. Ruiz, E.; Orozco, V.H.; Hoyos, L.M.; Giraldo, L.F. Study of sonication parameters on PLA nanoparticles preparation by simple emulsion-evaporation solvent technique. *Eur. Polym. J.* **2022**, *173*, 111307. [CrossRef]

31. Ekinci, M.; Yeğen, G.; Aksu, B.; İlem-Özdemir, D. Preparation and Evaluation of Poly(lactic acid)/Poly(vinyl alcohol) Nanoparticles Using the Quality by Design Approach. *ACS Omega* **2022**, *7*, 33793–33807. [CrossRef]
32. Kowalski, G.; Kijowska, K.; Witczak, M.; Kuterasiński, L.; Lukasiewicz, M. Synthesis and effect of structure on swelling properties of hydrogels based on high methylated pectin and acrylic polymers. *Polymers* **2019**, *11*, 114. [CrossRef]
33. Yoo, J.; Shin, M.; Rho, S.C.; Jung, M.; Seo, M. Hydrophobically modified poly(acrylic acid) coatings on silicone hydrogel contact lenses. *RSC Appl. Polym.* **2026**, *4*, 1355–1361. [CrossRef]
34. Xiao, Q.; Levine, M.S.; Iverson, B.L. Rethinking the Terms 'π-Stacking' and 'π–π Stacking' Again: A Proposal to Clarify the Language of Aromatic Interactions. *J. Am. Chem. Soc.* **2026**, *148*, 15331–15340. [CrossRef]
35. Xue, S.; Tan, W.; Mao, S.; Pan, H.; Ye, X.; Donlao, N.; Tian, J. Polyphenol-Based Functional Materials: Structural Insights, Composite Strategies, and Biomedical Applications. *Adv. Sci.* **2025**, *12*, e08924. [CrossRef]
36. Lee, H.; Dehez, F.; Chipot, C.; Lim, H.K.; Kim, H. Enthalpy-Entropy Interplay in π-Stacking Interaction of Benzene Dimer in Water. *J. Chem. Theory Comput.* **2019**, *15*, 1538–1545. [CrossRef]
37. Paik, D.; Lee, H.; Kim, H.; Choi, J.M. Thermodynamics of π–π Interactions of Benzene and Phenol in Water. *Int. J. Mol. Sci.* **2022**, *23*, 9811. [CrossRef]
38. Jiang, Z.; Chen, Q.; Yang, H. Drug delivery strategies for neuroprotective therapy in ischemic stroke: Application of nanotechnology. *Neural Regen. Res.* **2026**, *21*, 1793–1808. [CrossRef]
39. Peng, B.; Mohammed, F.S.; Tang, X.; Liu, J.; Sheth, K.N.; Zhou, J. Nanotechnology approaches to drug delivery for the treatment of ischemic stroke. *Bioact. Mater.* **2025**, *43*, 145–161. [CrossRef]
40. Yue, L.; Wang, M.; Khan, I.M.; Niazi, S.; Wang, B.; Ma, X.; Wang, Z.; Xia, W. Preparation and characterization of chitosan oligosaccharide derivatives containing cinnamyl moieties with enhanced antibacterial activities. *LWT* **2021**, *147*, 111663. [CrossRef]
41. Li, B.; Cui, J.; Xu, T.; Xu, Y.; Long, M.; Li, J.; Liu, M.; Yang, T.; Du, Y.; Xu, Q. Advances in the preparation, characterization, and biological functions of chitosan oligosaccharide derivatives: A review. *Carbohydr. Polym.* **2024**, *332*, 121914. [CrossRef]
42. Sánchez-Machado, D.I.; López-Cervantes, J.; Escárcega-Galaz, A.A.; Campas-Baypoli, O.N.; Martínez-Ibarra, D.M.; Rascón-León, S. Measurement of the degree of deacetylation in chitosan films by FTIR, 1H NMR and UV spectrophotometry. *MethodsX* **2024**, *12*, 102583. [CrossRef]
43. Pestov, A.; Nazirov, A.; Modin, E.; Mironenko, A.; Bratskaya, S. Mechanism of Au(III) reduction by chitosan: Comprehensive study with 13C and 1H NMR analysis of chitosan degradation products. *Carbohydr. Polym.* **2015**, *117*, 70–77. [CrossRef]
44. Lawrie, G.; Keen, I.; Drew, B.; Chandler-Temple, A.; Rintoul, L.; Fredericks, P.; Grøndahl, L. Interactions between alginate and chitosan biopolymers characterized using FTIR and XPS. *Biomacromolecules* **2007**, *8*, 2533–2541. [CrossRef]
45. Amaral, I.F.; Granja, P.L.; Barbosa, M.A. Chemical modification of chitosan by phosphorylation: An XPS, FT-IR and SEM study. *J. Biomater. Sci. Polym. Ed.* **2005**, *16*, 1575–1593. [CrossRef]
46. Sun, Y.; Kunc, F.; Balhara, V.; Coleman, B.; Kodra, O.; Raza, M.; Chen, M.; Brinkmann, A.; Lopinski, G.P.; Johnston, L.J. Quantification of amine functional groups on silica nanoparticles: A multi-method approach. *Nanoscale Adv.* **2019**, *1*, 1598–1607. [CrossRef]
47. Samrot, A.V.; Faradjeva, E.; Mohamed, A.A.; Sean, T.C.; Norbert, E.; Ng, X.Q.; Mun, C.Y.; Sze, C.H.; Arif, A.; Jie, L.S.; et al. Extraction, Purification, Characterization, Applications of Chitosan, Plant Gum Polysaccharides, and Other Polysaccharides: A Review. *Scientifica* **2025**, *2025*, 9919005. [CrossRef]
48. Ahmed Ismail, K.; El Askary, A.; Farea, M.; Awwad, N.S.; Ibrahium, H.A.; Moustapha, M.E.; Menazea, A. Perspectives on composite films of chitosan-based natural products (Ginger, Curcumin, and Cinnamon) as biomaterials for wound dressing. *Arab. J. Chem.* **2022**, *15*, 103716. [CrossRef]
49. Hamrayev, H.; Shameli, K. Synthesis and Characterization of Ionically Cross-Linked Chitosan Nanoparticles. *J. Res. Nanosci. Nanotechnol.* **2023**, *7*, 7–13. [CrossRef]
50. Sathiyabama, M.; Boomija, R.V.; Muthukumar, S.; Gandhi, M.; Salma, S.; Prinsha, T.K.; Rengasamy, B. Green synthesis of chitosan nanoparticles using tea extract and its antimicrobial activity against economically important phytopathogens of rice. *Sci. Rep.* **2024**, *14*, 7381. [CrossRef]
51. Kaur, M.; Singh, S.; Kaur, A. Structural changes in amide I and amide II regions of PCOS women analyzed by ATR-FTIR spectroscopy. *Heliyon* **2024**, *10*, e33494. [CrossRef]
52. Hasan, N.S.A.; Mohamad, S.; Mohamad, S.F.S.; Arzmi, M.H.; Supian, N.N.I. Ex-Situ Development and Characterization of Composite Film Based on Bacterial Cellulose Derived from Oil Palm Frond Juice and Chitosan as Food Packaging. *Pertanika J. Sci. Technol.* **2023**, *31*, 1173–1187. [CrossRef]
53. Claverie, E.; Perini, M.; Onderwater, R.C.A.; Pianezze, S.; Larcher, R.; Roosa, S.; Yada, B.; Wattiez, R. Multiple Technology Approach Based on Stable Isotope Ratio Analysis, Fourier Transform Infrared Spectrometry and Thermogravimetric Analysis to Ensure the Fungal Origin of the Chitosan. *Molecules* **2023**, *28*, 4324. [CrossRef]
54. Zhang, G.; Li, T.; Liu, J.; Wu, X.; Yi, H. Cinnamaldehyde-Contained Polymers and Their Biomedical Applications. *Polymers* **2023**, *15*, 1517. [CrossRef]

55. Sahu, D.; Verma, D.N.K. Synthesis and Biological Significance of Dibenzalacetone and its Derivatives as Bioactive α,β-Unsaturated Carbonyl Compounds. *Int. J. Creat. Open Res. Eng. Manag.* **2026**, *02*, 1–9. [CrossRef]
56. Hassan, M.A.; Abd El-Aziz, S.; Nabil-Adam, A.; Tamer, T.M. Formulation of novel bioactive gelatin inspired by cinnamaldehyde for combating multi-drug resistant bacteria: Characterization, molecular docking, pharmacokinetic analyses, and in vitro assessments. *Int. J. Pharm.* **2024**, *652*, 123827. [CrossRef]
57. Chen, H.; Hu, X.; Chen, E.; Wu, S.; McClements, D.J.; Liu, S.; Li, B.; Li, Y. Preparation, characterization, and properties of chitosan films with cinnamaldehyde nanoemulsions. *Food Hydrocoll.* **2016**, *61*, 662–671. [CrossRef]
58. Cui, R.; Liu, F.Y.; Wu, H. Enhancement of antibacterial activity of cinnamaldehyde against Bacillus cereus by nanoemulsion and its application in milk. *Food Biosci.* **2025**, *64*, 105931. [CrossRef]
59. Peng, J.; Song, X.; Yu, W.; Pan, Y.; Zhang, Y.; Jian, H.; He, B. The role and mechanism of cinnamaldehyde in cancer. *J. Food Drug Anal.* **2024**, *32*, 140–154. [CrossRef]
60. Higueras, L.; López-Carballo, G.; Gavara, R.; Hernández-Muñoz, P. Reversible Covalent Immobilization of Cinnamaldehyde on Chitosan Films via Schiff Base Formation and Their Application in Active Food Packaging. *Food Bioprocess Technol.* **2015**, *8*, 526–538. [CrossRef]
61. Taha, A.G.; Hussein, M.K.; Hezma, A.M.; Dardeer, H.M.; Aly, M.F. Synthesis, Characterization, and Antibacterial Performance of Chitosan–Cinnamaldehyde Nanoparticles. *J. Inorg. Organomet. Polym. Mater.* **2026**. [CrossRef]
62. Sultan, M.; Youssef, A.M.; Taha, G. Potential antimicrobial cotton fabrics treated with cinnamaldehyde/chitosan-alginate nanocapsules for food packaging purposes. *Int. J. Biol. Macromol.* **2024**, *279*, 135384. [CrossRef]
63. Pereira, A.G.B.; Muniz, E.C.; Hsieh, Y.L. 1H NMR and 1H-13C HSQC surface characterization of chitosan-chitin sheath-core nanowhiskers. *Carbohydr. Polym.* **2015**, *123*, 46–52. [CrossRef]
64. Cheng, Q.; Widanage, M.C.D.; Yarava, J.R.; Ankur, A.; Latgé, J.-P.; Wang, P.; Wang, T. Molecular architecture of chitin and chitosan-dominated cell walls in zygomycetous fungal pathogens by solid-state NMR. *Nat. Commun.* **2024**, *15*, 8295. [CrossRef]
65. Ren, G.; Clancy, C.; Tamer, T.M.; Schaller, B.; Walker, G.M.; Collins, M.N. Cinnamyl O-amine functionalized chitosan as a new excipient in direct compressed tablets with improved drug delivery. *Int. J. Biol. Macromol.* **2019**, *141*, 936–946. [CrossRef]
66. Tamer, T.M.; Hassan, M.A.; Omer, A.M.; Valachová, K.; Eldin, M.S.M.; Collins, M.N.; Šoltés, L. Antibacterial and antioxidative activity of O-amine functionalized chitosan. *Carbohydr. Polym.* **2017**, *169*, 441–450. [CrossRef]
67. Tozaki, H.; Odoriba, T.; Okada, N.; Fujita, T.; Terabe, A.; Suzuki, T.; Okabe, S.; Muranishi, S.; Yamamoto, A. Chitosan capsules for colon-specific drug delivery: Enhanced localization of 5-aminosalicylic acid in the large intestine accelerates healing of TNBS-induced colitis in rats. *J. Control Release* **2002**, *82*, 51–61. [CrossRef]
68. Yue, L.; Sun, D.; Mahmood Khan, I.; Liu, X.; Jiang, Q.; Xia, W. Cinnamyl alcohol modified chitosan oligosaccharide for enhancing antimicrobial activity. *Food Chem.* **2020**, *309*, 125513. [CrossRef]
69. Razavifar, M.; Abdi, A.; Nikooee, E.; Aghili, O.; Riazi, M. Quantifying the impact of surface roughness on contact angle dynamics under varying conditions. *Sci. Rep.* **2025**, *15*, 16611. [CrossRef]
70. Jagodzińska, S.; Pałys, B.; Wawro, D. Effect of chitosan film surface structure on the contact angle. *Prog. Chem. Appl. Chitin Its Deriv.* **2021**, *26*, 89–100. [CrossRef]
71. Gül, L.B.; Akgün, A.; Gül, O. Nanoencapsulation of Royal Jelly in Chitosan Nanocomplex through Ionic Gelation: Optimization and Characterization. *Food Biophys.* **2026**, *21*, 20. [CrossRef]
72. Sethunga, M.; Rangani, S.C.; Munaweera, I.; Ranaweera, K.K.D.S. Hybrid nanoencapsulation systems: Integrating natural polymers with synthetic nanomaterials for enhanced delivery of bioactive compounds in functional foods. *Nanoscale Adv.* **2025**, *7*, 7867–7890. [CrossRef]
73. Silva, N.C.; Chevigny, C.; Domenek, S.; Almeida, G.; Assis, O.B.G.; Martelli-Tosi, M. Nanoencapsulation of active compounds in chitosan by ionic gelation: Physicochemical, active properties and application in packaging. *Food Chem.* **2025**, *463*, 141129. [CrossRef]
74. Ulici, A.M.; Găină-Gardiuta, A.; Vodnar, D.; Barbu-Tudoran, L.; Podea, P.V. Nanoencapsulation of citrus essential oils in systematic modified chitosan-based nanofibers. *J. Appl. Polym. Sci.* **2024**, *141*, e56176. [CrossRef]
75. Riccucci, G.; Ferraris, S.; Reggio, C.; Bosso, A.; Örlygsson, G.; Ng, C.H.; Spriano, S. Polyphenols from Grape Pomace: Functionalization of Chitosan-Coated Hydroxyapatite for Modulated Swelling and Release of Polyphenols. *Langmuir* **2021**, *37*, 14793–14804. [CrossRef]
76. Nguyen, T.T.; Pham, B.T.T.; Le, H.N.; Bach, L.G.; Thuc, C.N.H. Comparative characterization and release study of edible films of chitosan and natural extracts. *Food Packag. Shelf Life* **2022**, *32*, 100830. [CrossRef]
77. Talón, E.; Trifkovic, K.T.; Vargas, M.; Chiralt, A.; González-Martínez, C. Release of polyphenols from starch-chitosan based films containing thyme extract. *Carbohydr. Polym.* **2017**, *175*, 122–130. [CrossRef]
78. Wiggers, H.J.; Chevallier, P.; Copes, F.; Simch, F.H.; Veloso, F.d.S.; Genevro, G.M.; Mantovani, D. Quercetin-Crosslinked Chitosan Films for Controlled Release of Antimicrobial Drugs. *Front. Bioeng. Biotechnol.* **2022**, *10*, 814162. [CrossRef]

79. Dai, Z.; Yin, W.; Li, J.; Ma, L.; Chen, F.; Shen, Q.; Hu, X.; Xue, Y.; Ji, J. Zein and Trimethyl Chitosan-Based Core–Shell Nanoparticles for Quercetin Oral Delivery to Enhance Absorption by Paracellular Pathway in Obesity Mice. *Biomater. Res.* **2025**, *29*, 0193. [CrossRef]
80. Geng, F.; Zhang, M.; Sun, T.; Xie, J.; Gan, J.; Li, X.; Xue, B. Effect of molecular weight of chitosan on quercetin-loaded chitosan nanoparticles. *J. Sci. Food Agric.* **2024**, *104*, 9531–9539. [CrossRef]
81. Hao, J.; Guo, B.; Yu, S.; Zhang, W.; Zhang, D.; Wang, J.; Wang, Y. Encapsulation of the flavonoid quercetin with chitosan-coated nano-liposomes. *LWT* **2017**, *85*, 37–44. [CrossRef]
82. Carrasco-Sandoval, J.; Aranda, M.; Henríquez-Aedo, K.; Fernández, M.; López-Rubio, A.; Fabra, M.J. Impact of molecular weight and deacetylation degree of chitosan on the bioaccessibility of quercetin encapsulated in alginate/chitosan-coated zein nanoparticles. *Int. J. Biol. Macromol.* **2023**, *242*, 124876. [CrossRef]
83. Mu, D.; Zhou, L.; Shi, L.; Liu, T.; Guo, Y.; Chen, H.; Luo, H.; Ma, J.; Zhang, H.; Xiong, P.; et al. Quercetin-crosslinked chitosan nanoparticles: A potential treatment for allergic rhinitis. *Sci. Rep.* **2024**, *14*, 4021. [CrossRef]
84. Roy, S.; Rhim, J.W. Fabrication of chitosan-based functional nanocomposite films: Effect of quercetin-loaded chitosan nanoparticles. *Food Hydrocoll.* **2021**, *121*, 107065. [CrossRef]
85. Liu, J.; Yu, H.; Kong, J.; Ge, X.; Sun, Y.; Mao, M.; Wang, D.Y.; Wang, Y. Preparation, characterization, stability, and controlled release of chitosan-coated zein/shellac nanoparticles for the delivery of quercetin. *Food Chem.* **2024**, *444*, 138634. [CrossRef]
86. Nalini, T.; Basha, S.K.; Sadiq, A.M.; Kumari, V.S. In vitro cytocompatibility assessment and antibacterial effects of quercetin encapsulated alginate/chitosan nanoparticle. *Int. J. Biol. Macromol.* **2022**, *219*, 304–311. [CrossRef]
87. Poznanski, P.; Hameed, A.; Orczyk, W. Chitosan and Chitosan Nanoparticles: Parameters Enhancing Antifungal Activity. *Molecules* **2023**, *28*, 2996. [CrossRef]
88. Lawson, M.K. Improvement of Therapeutic Value of Quercetin with Chitosan Nanoparticle Delivery Systems and Potential Applications. *Int. J. Mol. Sci.* **2023**, *24*, 3293. [CrossRef]
89. Panbhukarasu, S.; Vijayalekha, A.; Natarajan, K.; Anandasadagopan, S.K.; Pandurangan, A.K. Integrated network pharmacology and bio-functional chitosan-hydroxyapatite scaffolds incorporating quercetin for enhanced bone regeneration in articular cartilage defects. *J. Bioact. Compat. Polym.* **2025**, *40*, 248–266. [CrossRef]
90. Larijani, G.; Lotfi, A.; Barati, S.; Janzadeh, A.; Abediankenari, S.; Faghihi, F.; Amini, N. The effect of chitosan/alginate hydrogel loaded quercetin on wound healing in diabetic rat model. *J. Mol. Histol.* **2025**, *56*, 225. [CrossRef]
91. Sudhakar, M.P.; Nived, S.A.; Dharani, G. Fabrication and Characterization of Agar- and Seaweed-Derived Biomembrane Films for Biomedical and Other Applications. *Biopolymers* **2025**, *116*, e23643. [CrossRef]
92. Alishahi, M.; Xiao, R.; Kreismanis, M.; Chowdhury, R.; Aboelkheir, M.; Lopez, S.; Altier, C.; Bonassar, L.J.; Shen, H.; Uyar, T. Antibacterial, Anti-Inflammatory, and Antioxidant Cotton-Based Wound Dressing Coated with Chitosan/Cyclodextrin-Quercetin Inclusion Complex Nanofibers. *ACS Appl. Bio Mater.* **2024**, *7*, 5662–5678. [CrossRef]
93. Liu, F.; Liu, Y.; Guo, Y.; Liu, J.; Dong, J.; Wang, T.; Hao, D.; Zhang, Y. FTIR determination of the degree of molar substitution for hydroxypropyl chitosan. *Carbohydr. Polym.* **2024**, *339*, 122229. [CrossRef]
94. Carpintero, M.; Marcet, I.; Cortizo, C.; Guerrero, P.; de la Caba, K.; Rendueles, M.; Díaz, M. Chitosan modification with octenyl succinic anhydride (OSA): Effect of the degree of substitution on the structural, mechanical and barrier properties in the synthetized bioplastics. *Food Hydrocoll.* **2026**, *171*, 111838. [CrossRef]

Disclaimer/Publisher's Note: The statements, opinions and data contained in all publications are solely those of the individual author(s) and contributor(s) and not of MDPI and/or the editor(s). MDPI and/or the editor(s) disclaim responsibility for any injury to people or property resulting from any ideas, methods, instructions or products referred to in the content.